*Geophys. J. Int.* (1996) **125,** 73–94

# A tensile, flexural model for the initiation of subduction

David V. Kemp[1] and David J. Stevenson[2]

[1] *Seismological Laboratory,* 252-21, *California Institute of Technology, Pasadena,* CA 91125, *USA*

[2] *Division of Geological and Planetary Sciences,* 170-25, *California Institute of Technology, Pasadena,* CA 91125, *USA*

Accepted 1995 October 11. Received 1995 October 10; in original form 1994 December 5

## SUMMARY

We argue that subduction may be initiated at passive continental margins without shortening the lithosphere. Overcoming the lithosphere's high compressive strength requires special circumstances, and these make it difficult to explain the nearly complete recycling of old sea-floor. Instead, we present a model that predicts tensile decoupling of the continental and oceanic lithosphere, passive rifting, and foundering of the sea-floor beneath material welling up in the rift. This occurs because the lithosphere in a new ocean basin establishes mechanical continuity with the continent at a depth comparable to mid-ocean ridges. Later subsidence at the margin is therefore inhibited by flexure, which implies shear stresses that promote fault slip and tensile stresses necessary to balance the component of the plate's weight directed down the margin slope. We show that this tension can more than offset ridge push. In our model, an important additional tension arises from basal shear tractions resisting the plate's motion away from the mid-ocean ridge, although these tractions cannot be evaluated with confidence. Slip on a high-angle fault decouples the oceanic and continental lithosphere when shear stresses arising from flexure and the applied tension exceed the lithosphere's shear strength under these loads. A passive rift then forms, allowing a mantle column to rise to the height of mid-ocean ridges, over 3 km above the old sea-floor, and flow onto the surface in a gravity current. This load flexes the plate downwards, which enhances the flow and lets the old oceanic lithosphere founder.

This model is consistent with the presence of oceanic material in continental forearcs and the youth of ophiolites when they are obducted, as both might be explained by rifting a margin and underthrusting the juvenile crust formed there. Boninites in ophiolite complexes and tectonites at their bases show depleted and hydrated geochemistries consistent with the melting of rifted mantle lithosphere that receives volatiles from foundering oceanic crust.

**Key words:** continental margins, flexure of the lithosphere, ophiolites, rifts, stress distribution, subduction.

## 1 INTRODUCTION

The central role of subduction in tectonics and mantle dynamics has been recognized for many years, but the means by which new subduction zones are created have not been clearly established. Conductive cooling makes oceanic lithosphere gravitationally unstable (i.e. more dense than the underlying mantle when taken adiabatically to the same pressure) within ~50 Myr (Oxburgh & Parmentier 1977; Molnar & Atwater 1978; England & Wortel 1980; Sacks 1983; Davies 1992), but this is not a sufficient condition for subduction, as shown by the existence of lithosphere with ages of 100 to 200 Myr. The boundary layer acquires a high viscosity and finite brittle strength along with its anomalous density, and these inhibit descent. Mechanisms for initiating subduction, the self-sustained release of the lithosphere's buoyancy, have proven difficult to identify. We are concerned here with mechanisms for the initiation of subduction on an earth where subduction already takes place, avoiding the more difficult problem of initiating subduction on a planet where there is not any.

The forces resisting subduction and the driving forces that might overcome them have been investigated by a number of workers. McKenzie (1977) considered the resistance offered by fault friction and the downgoing plate's bending strength and balanced these by density moment forces, or 'ridge push,' and the pull of an incipient slab. He estimated that a slab's descent would become self-sustaining if external forces pushed the leading edge to a depth of ~180 km, but he was unable to explain how such a finite-amplitude instability could be formed.

Passive continental margins have been considered likely

settings for initiation because such sites would fit into the classic Wilson cycle (Wilson 1966), old, thick lithosphere exists there (Dewey & Bird 1970), margins are crustal interfaces at which previous faulting has occurred (Karig 1982), and because abundant sediments load them that might overcome the lithosphere's strength (Dietz 1963; Dewey 1969; Cohen 1982). Cloetingh and co-workers (Cloetingh & Wortel 1982; Cloetingh, Wortel & Vlaar 1982a,b, 1984, 1989) have investigated margins at which sedimentation keeps up with lithospheric subsidence, or is augmented, as at a river delta, and examined the conditions under which such loading might help initiate subduction. The sediments induce flexure at the margin and contribute, along with ridge push and isostasy, to the overall state of stress. Lithospheric failure was taken to occur when the stresses exceed the strength of the materials at all depths. The authors concluded that because the strong brittle/elastic layer thickens with time, as does the sediment load, complete failure cannot be induced except by applying the maximum load to young ($\sim$20 Myr) margins; the increased negative buoyancy and loading of old margins did not make them more prone to failure in these models. Erickson (1993) argued that, in special circumstances, margin flexure might be described by a semi-infinite oceanic plate on which sedimentation keeps up with subsidence, leading to the prediction that the plate surface can reach depths of 35 km. He further argued that the top of the oceanic plate might then be adjacent to the base of the continent's brittle/elastic layer. It is not clear, however, that the continent's elastic layer would be unable to track downwards with the sea-floor through heat conduction, making a depressed margin as resistant to ridge push as an undisturbed one.

A number of other settings have been suggested as sites for initiation, but Mueller & Phillips (1991) evaluated lithospheric strengths at several—normal oceanic lithosphere, passive margins, transforms, fracture zones and spreading centres—and found that compressive failure driven by ridge push should not be expected at any of these.

These difficulties in initiating subduction have led to several appeals to special circumstances. Erickson (1993) and Erickson & Arkani-Hamed (1993) argued that fluid pressures exceeding hydrostatic levels, the reheating of a margin by a passing mantle plume, or an absence of hydrothermal circulation to cool sediments could be important weakening mechanisms in certain cases. They also discussed a transform that is oblique to the current ridge push due to a change in spreading directions, noting that if the transform were reactivated, it would tend to decouple the margin on one side of the transform/margin intersection. Mueller & Phillips (1991) argued that new subduction zones are created by 'trench congestion' events, based on models that relate buckling in the Indian Ocean to the India–Asia collision (McAdoo & Sandwell 1985; Cloetingh & Wortel 1986; Zuber 1987), on the lithosphere-scale thrusting that appears to be taking place where the Izu–Ogasawara arc collides with Japan (Chamot-Rooke & Le Pichon 1989), and on seismic data from the New Hebrides, Santa Cruz, and Solomon trenches (Kroenke & Walker 1986; Okal, Woods & Lay 1986). Pulses of tectonic stress associated with broader plate reorganizations have also been called upon (Erickson & Arkani-Hamed 1993).

Major tectonic events, such as the India–Asia collision, and complex plate interactions, as in the western Pacific, do appear to cause polarity reversals, trench jumps and along-strike propagation of existing subduction zones. The structures of the Arctic, Atlantic, Southern, and western Indian Ocean basins may be more historically representative, however, which would significantly limit the influence of these processes. In any case, these processes modify subduction patterns in a basin that is being consumed, rather than start a basin's consumption. Mueller & Phillips (1991) addressed this issue by proposing that a basin with no subduction zones might be 'infected' with one from an adjoining basin and then be consumed through a series of intrabasin trench reorganizations. But notably, only 0.001 per cent of the total volume of Phanerozoic ocean crust has been emplaced as ophiolites (Coleman 1977), thereby avoiding subduction, and no crust older than $\sim$200 Myr survives in the modern oceans. This would appear to limit the degree to which basin evolution can depend on external tectonic events or otherwise fail to be self-determined. Thus, while a variety of processes may locally promote margin failure or redistribute subduction zones, we believe that a passive margin model, in which the physics of basin evolution provides a prescription for its demise, offers the most plausible explanation for the remarkably efficient recycling of old oceanic lithosphere.

Two features of previous passive margin models, however, require re-examination. First, sediment loads and the flexure they induce can give stresses that exceed the lithosphere's strength throughout, but, because the sign of the longitudinal stress changes with depth, do not by themselves lead to coherent slip of one plate over another (Mueller & Phillips 1991). Secondly, Cloetingh *et al.* (1989 and previous work) took the subsidence rate of the oceanic lithosphere at the margin from a sediment-loaded boundary-layer cooling model (Turcotte & Ahern 1977). Presumably it was believed that maximizing the volume of sediments, as this model does, would maximize their potential for initiating subduction. The difficulty is that the oceanic lithosphere adjacent to the continent was assumed to subside freely when defining the sedimentary basin (Fig. 1a), but was taken to be mechanically bound to the continent before applying a sediment load appropriate for the margin's age. This is not self-consistent with respect to the mechanical continuity of the margin.

We believe that a more physical model would have the oceanic lithosphere formed at a new passive margin weld onto the continent at a depth comparable to mid-ocean ridges and immediately establish mechanical continuity with the continental lithosphere. In this case, subsidence on the oceanic side of the margin is inhibited by the flexural response of the plate, as shown schematically in Fig. 1(b). The shear strength of the lithosphere prevents it from subsiding to its depth of compensation. Compelling evidence for this sort of behaviour was provided by Steckler & Watts (1982) who examined North America's Atlantic margin and found that the sediments on the outer continental shelf tilt seawards and successively onlap onto the coastal plain, and that both of these relationships can be explained by a model in which the lithosphere is flexurally coupled at all post-rift times. In addition, Rabinowitz & LaBrecque (1977) studied Airy-corrected gravity data along three passive-margin profiles where seismic constraints were available, finding that a gravity low is obtained on the continental side with a corresponding high on the oceanic side. Rabinowitz (1982) found that this pattern is a common feature of passive margins, further supporting an early mechanical coupling and flexural evolution.

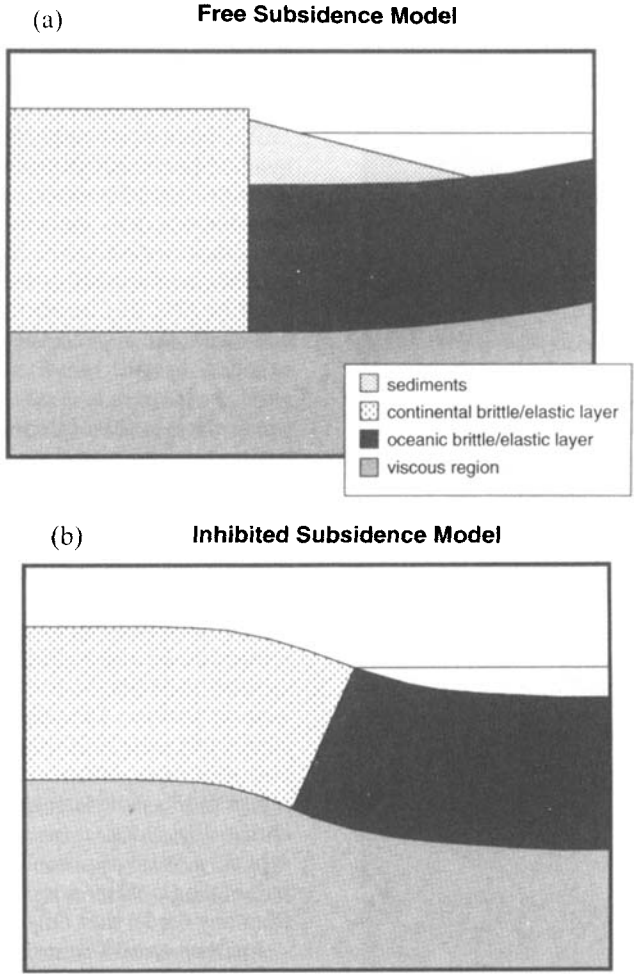


**Figure 1.** Margin subsidence models. (a) Previous models assumed the oceanic lithosphere subsides freely when defining sediment loads, but took it to be mechanically bound to the continent when computing the flexural response. (b) Model in which oceanic subsidence is inhibited by the shear strength of the lithosphere, leading to a flexural profile, even in the absence of sedimentation.

Another assumption in previous studies has been that subduction zones are contractional features from their inception. The focus, therefore, has been on identifying sources of compressive stress capable of driving slip on a thrust fault that cuts the lithosphere. But it is well known that the lithosphere is weaker in tension than compression (e.g. Brace & Kohlstedt 1980). This asymmetry arises because an applied tensile traction partly offsets the lithostatic pressure acting on faults, thereby reducing the maximum shear stress that can be supported by fault friction. Conversely, applied compressive stresses strengthen faults. Erickson (1993) and Erickson & Arkani-Hamed (1993) discussed this with regard to initiation at the continental termination of a transform, noting that if it were reactivated, the resulting tension would tend to locally decouple the margin. Their model, however, depends on a site-specific geometry, and it is not clear that the response to the decoupling they predict would be greater than local isostatic adjustment. Turcotte, Haxby & Ockendon (1977) suggested that the initial failure leading to subduction could be tensile, but no model has been proposed that predicts tensile passive margin failure under reasonably common or predictable circumstances.

Below we will consider a margin that experiences both flexure and an applied tension and investigate the possibility that the initial failure is a high-angle normal fault. In our model, this fault decouples the oceanic and continental lithosphere allowing a passive rift to develop. We later discuss how the juxtaposition of the rift and old oceanic lithosphere can allow the lithosphere to founder. Subduction would then be initiated by the sinking old lithosphere and ridge push.

## 2 A TENSILE, FLEXURAL MODEL FOR INITIATION

### 2.1 A new scenario

In light of the flexure at passive margins due to inhibited subsidence and the relative weakness of the lithosphere in tension, we propose that the following sequence of events leads to passive margin failure and the initiation of subduction. Quantitative arguments follow.

In the initial stage (Fig. 2a), a plate comprising both continental and oceanic lithosphere is dragged towards the continent by subduction-induced flow under its leading edge—the so-called trench suction—and is driven by ridge push. South America provides a modern example of the geometry. The corner flow induced by the downgoing slab applies a trench-directed shear traction to the base of the continent and, by

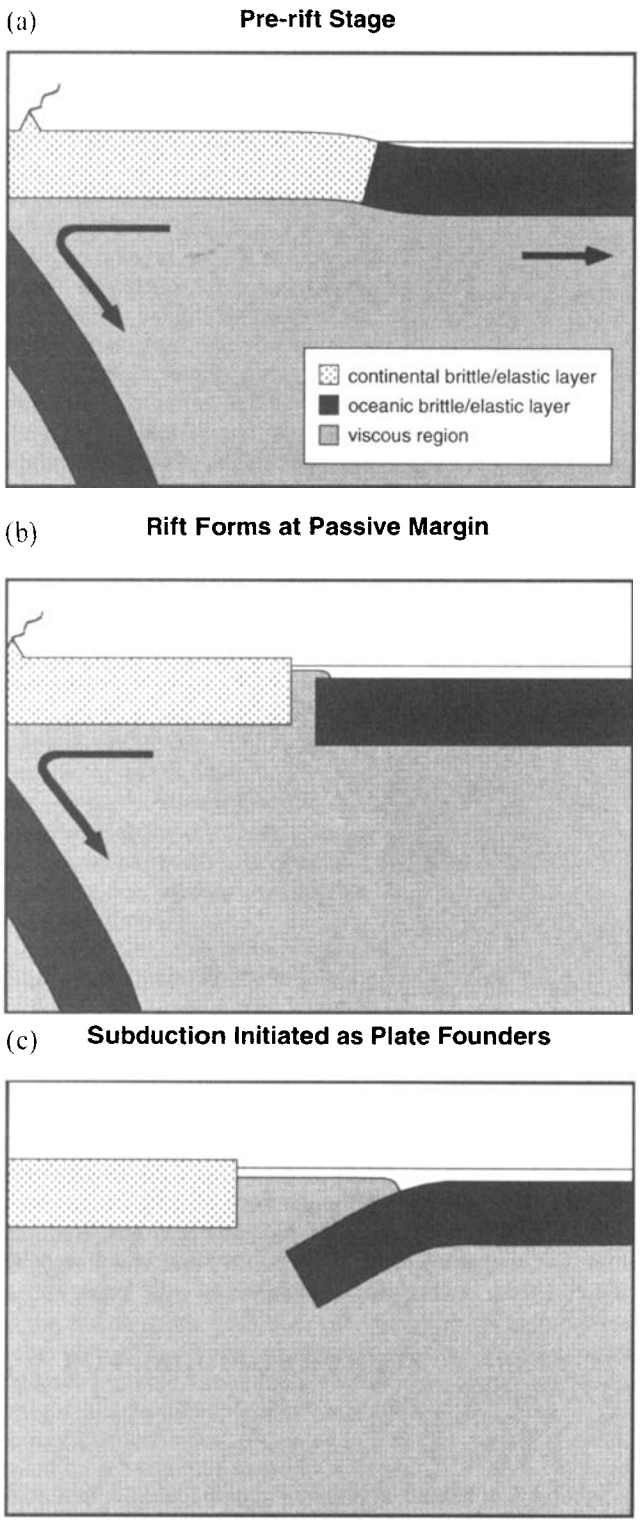


**Figure 2.** A new initiation scenario. Surficial layers represent the brittle/elastic portion of the lithosphere that can support stresses on long time-scales. (a) A plate comprising continental and oceanic lithosphere, with a flexed passive margin, experiences basal tractions associated with subduction and sea-floor spreading. (b) Shear stresses exceed the shear strength of the margin under tension arising from the margin's slope and basal tractions. The oceanic and continental lithosphere decouple, leading to a passive rift. (c) A gravity current flows onto the old seafloor causing it to flex downwards and founder.

stress equilibrium, makes a tensile contribution to the horizontal normal stress in the overriding plate. However, the corner flow dies off rapidly with distance (Batchelor 1967; Stevenson & Turner 1977; Tovish, Schubert & Luyendyk 1978). If mid-ocean ridges are passive, as is generally supposed, much of the plate can be expected to experience a basal shear traction directed towards the ridge. That is, while the flow near the arc may lead the plate, driving it forward, further away the mantle beneath the plate will lag, being driven by its coupling to the rigid surface layer. If this correctly describes the flow field, the horizontal normal stress in the overriding plate will take a value at the trench defined by the interplate coupling, become more tensile over the region in which the basal shear stress is trench directed, and achieve a maximum tensile stress at some intermediate position. It will then become less tensile with increasing application of ridge-directed shear and eventually change to compression as the ridge is approached.

One way to explore the expected stress distribution is to consider the flow field that results purely kinematically for Fig. 2(a), assuming the non-subducting plate is at rest and is bounded on the right by a ridge. If the ridge is spreading symmetrically and migrating to the right, it creates a clockwise circulation, while the subducting slab creates a counterclockwise circulation. This allows the stress state within the non-subducting plate to become tensile even when the stresses near both the ridge and trench are likely to be compressive. We return to this issue later and develop an analytical, generalized corner-flow solution in the Appendix that demonstrates this explicitly. We recognize, however, that the actual flow will be part of the global mantle circulation and may differ significantly from any model that only considers the motions of two plates.

Another tensile contribution to the margin-normal stress arises from the inhibited subsidence and is required to balance the component of the plate's weight directed down the slope of the flexural profile. We will demonstrate below that this can be comparable to, or more than offset, ridge push.

Fault slip will take place at the margin, decoupling the oceanic and continental lithosphere, if the integrated shear stresses resolved onto any surface exceed its shear strength under the applied tension. If this happens, the continent will be dragged away from the oceanic lithosphere by the pre-existing driving forces, and a passive rift will form between the continent and old sea-floor (Fig. 2b). Once separated, the oceanic lithosphere adjacent to the rift will subside to its compensation depth, over 3 km deeper than a mid-ocean ridge. The static pressure field beneath the rift, therefore, will be capable of driving hot mantle to a comparable height above the old sea-floor. Partially molten mantle material will then flow out onto the plate surface in a gravity current, causing it to flex downwards. This will in turn increase the thickness and speed of the flow. Thus, the lithosphere adjacent to the rift will founder while experiencing an undiminished ridge push, and subduction will be initiated (Fig. 2c).

### 2.2 Supporting evidence

Before presenting a preliminary evaluation of the model physics, we note some observations that are consistent with the foregoing scenario. A first point is that there are at least two instances documented in the geological record of Atlantic-type margins being transformed directly to Andean type.

Stanistreet, Kukla & Henry (1991) synthesized the data on the structure and depositional palaeoenvironments adjacent to the Congo and Kalahari Cratons and found clear evidence that a rifting event separated the cratons and mature passive margin sequences developed. This was followed by closure of the intervening Khomas Sea, marked by growth of an accretionary prism at the edge of the Congo Craton and calc-alkaline magmatism that preceded collision of the cratons. Similarly, the development of the Hikurangi Trough off New Zealand is recorded in the change from marl and limestone sedimentation to the Early Miocene deposition of flysch and olistostromes at the onset of thrusting, but preceding calc-alkaline volcanism (Chanier & Ferrière 1991). In neither case is there an older arc that would indicate a reversal of subduction polarity. We do not specifically argue that subduction was initiated at these two margins by the mechanism we propose; we simply note the strong evidence that initiation has occurred at passive margins.

The early structural development of mature subduction zones is difficult to unravel, but some consequences of that history are consistent with the model outlined above. Forearc basins, for example, may commonly be underlain by either oceanic or stretched continental crust trapped in the initiation process (Dickinson & Seely 1979). Petrological data linking forearc basement to oceanic environments, even in several subduction zones at continental margins, led Mueller & Phillips (1991) to argue that initiation takes place in wholly intra-oceanic environments. We would argue, however, that these data are equally compatible with our continental margin model because an oceanic section would be entrapped when the old oceanic lithosphere is thrust beneath the juvenile crust formed in the rift.

Ophiolites also reflect the early development of subduction zones. Casey & Dewey (1984) presented intraoceanic initiation models based on the youth of ophiolites when they are obducted and evidence that obduction onto continents generally occurs at previously stable margins. These observations are again compatible with our model, however, if some of the crust formed in the rift were obducted as an ophiolite. In fact, Pearce, Lippard & Roberts (1984) identified a class of supra-subduction zone ophiolites, ones whose geochemistry reflects trace-element enrichment from an underlying slab, that 'are found in most, if not all, of the world's major Phanerozoic orogenic belts'. Despite the slab component, these ophiolites appear to result from spreading that *precedes* the onset of arc volcanism. In addition, they have ultramafic tectonites derived from a less fertile source or through higher degrees of partial melting than other, MORB-like ophiolites, consistent with hydration of previously depleted lithospheric mantle. Boninites in ophiolite complexes also reflect hydrous melting of a depleted source, as well as high temperatures ($\sim 1200\,^{\circ}C$) at shallow depths ($\sim 30$ km), as may occur in a rifting oceanic plate (Cameron, Nisbet & Dietrich 1979). Also, Hacker (1994) has obtained $^{40}Ar/^{39}Ar$ hornblende ages from the Samail ophiolite's metamorphic sole that demonstrate that the sole, 15–20 km deep in the section, was cooled below 525 °C within $\sim 1$ Myr of the crystallization age of late-stage plagiogranites. That is, the ophiolite was underthrust and chilled within $\sim 1$ Myr of its formation. Such an event is consistent with our initiation scenario, but would be improbable at mid-ocean or backarc spreading centres where old lithosphere is unavailable. While the details of passive margin rifting and the initial underthrusting (and thus the expected tectonic fabrics) are beyond the scope of this paper, our model does predict a rift involving depleted, lithospheric mantle, followed quickly by underthrusting of enriched, oceanic crust. The buoyancy of the juvenile rift crust relative to the adjacent old lithosphere would aid in its obduction as an ophiolite, and we would expect all this to occur before arc magmatism could be established.

Turning to the modern Earth, we note evidence that passive margins are not universally in compression due to ridge push, but can also exhibit margin-normal tension. In northeastern Brazil, for example, focal mechanisms are consistent with a component of margin-normal tension that is overwhelmed where the margin is normal to the ridge push direction, but gives margin-normal T-axes where the margin is oblique (Assumpção 1992). Similarly, Bungum *et al.* (1991) used data from regional seismic networks to identify stress domains in Norway and the adjacent basins. They found that these tended to be dominated by ridge push or identifiable tectonic features, but one domain on the Atlantic margin surprisingly gave T-axes that were nearly normal to both the margin and the mid-Atlantic ridge. A third seismic suggestion of margin-normal tension comes from the one CMT solution in the Harvard catalogue for the passive margins of Antarctica. This solution again gives a T-axis that is at a high angle to both the margin and the (Southeast Indian) ridge. The motion of the Antarctic plate in a hotspot reference frame (Gripp & Gordon 1990) is towards that edge of the continent, but the Australian plate also moves northwards and much more rapidly, which would tend to induce flow and tractions that would put that side of Antarctica in tension.

Another seismic observation may at first seem to contradict our model but is in fact consistent: intraoceanic seismicity does not yield normal-type focal mechanisms in lithosphere older than 35 Myr (Wiens & Stein 1984). One might conclude that no part of the older lithosphere experiences deviatoric tension, but the seismic expression of this tension would be spatially and temporally limited. The tension induced by ridge-directed basal shear equals the integrated traction divided by the mechanical thickness of the plate. A thin plate promotes failure near the ridge, but the maximum tension in older lithosphere will occur where the basal shear stress changes sign. Other factors aside, normal faulting away from the ridge will occur at this local maximum in tension rather than throughout the basin. If this peak falls within the continent, the margin will experience more tension than intraoceanic sites. The peak tension also increases with the size of the plate, which limits normal faulting to when the maximum reaches the strength of the lithosphere. Current levels of tension may simply fall below this threshold. Furthermore, slip in a compensated setting must be driven by the shear stress resolved onto the fault from the applied normal stress, whereas at the margin, flexure implies an additional shear stress and complements the tension with that resulting from the slope of the flexed margin. Normal faulting might therefore be expected at the margin before an intraoceanic site, but this depends on the flexural history and the flow field beneath the plate.

Borehole breakout data indicate margin-normal tension off eastern North America, but this has been explained by flexural extension of the upper crust due to sediment loading (Zoback 1992), i.e. by moments as opposed to uniform tension. These shallow observations, however, cannot exclude the latter possibility.

Clearly, these few observations do not represent an exhaustive review of the geological record or current stress indicators as they may bear on our model. But in our preliminary review, our model is consistent with the following: the marine petrological affinities of forearcs; important aspects of ophiolite evolution and petrology, including their youth when obducted, their apparent origins in marginal basins, the depleted nature of their tectonites, and boninitic magmatism; passive-margin and intraoceanic seismicity; and borehole breakout data. Additional observations related to the early stages of subduction may well have been interpreted with a prejudice towards initial contraction, while dykes and other indicators of extension may be erroneously associated with the basin's initial rifting event, with crust formed at mid-ocean ridges, or with later-stage backarc environments. While modern observations indicate the predominance of intraplate compression in the upper crust (Zoback *et al.* 1989; Zoback 1992), deviations occur at passive margins that have been attributed to flexure due to sediment loading (Stein *et al.* 1989), but these could also indicate a component of uniform tension. Inferences about modern stresses must be used cautiously in any case because initiation may be fairly rare. Jarrard's (1986) review of modern subduction zones lists 39 active arc segments, none of which is younger than 6 Myr. Also, subduction zones from the New Hebrides to the Philippines might best be considered reorganizations of subduction in a region with much older trenches (e.g. Southwest Japan, which has been active since 175 Myr), and the Aegean might be considered an extension of preceding Alpine events. In this view, no distinct and currently active subduction zones have formed for at least 20 Myr. Thus, no modern passive margin need be at the point in the Wilson cycle where it experiences tension, and our model suggests that currently compressive margins can become more tensile with time.

### 2.3 Margin flexure

To determine whether the above scenario is feasible, we now turn to the flexural evolution of a simplified passive margin. We assume that the boundary between continental and oceanic lithosphere is sharp and that the margin is sediment free. Margins often include a stretched wedge of continental crust that gives them a more complex density distribution, but we only want to examine the generalized behaviour. The omission of a sediment load on the oceanic side of the margin gives a highly conservative estimate of the flexure, as sediments can independently add on the order of 100 MPa to the internal shear stresses (e.g. Cloetingh & Wortel 1982; Cloetingh *et al.* 1989; Stein *et al.* 1989). Also, sediments are usually considered strengthless themselves, but insulate the underlying material, thereby thinning the layer that is cool enough to support stresses. We use a plate model (Langseth, Le Pichon & Ewing 1966; McKenzie 1967) to provide a convenient average characterization of oceanic lithosphere's thermal evolution, and in our model, the density anomaly driving the initial fault motion will not diffuse away if the slip rate is small (*cf.* McKenzie 1977; Mueller & Phillips 1991), so we only concern ourselves with the brittle/elastic layer that can support stresses indefinitely. We assume that stresses relax in the underlying material. Given these assumptions, the margin responds flexurally according to

$$D_c \frac{d^4 w}{dx^4} + \rho_m g w = 0; \qquad x < 0, \tag{1}$$

$$D_o \frac{d^4 w}{dx^4} + (\rho_m - \rho_w) g w = 0; \qquad x \geq 0, \tag{2}$$

where the $D$'s represent the continental and oceanic flexural rigidities, $x$ measures horizontal distance, $w$ is the upward deflection from the compensation depth, $\rho$'s represent the mantle and seawater densities, and $g$ is the gravitational acceleration. See Table 1 for a list of symbols. As the oceanic lithosphere cools, the compensation depth becomes increasingly discontinuous at $x = 0$, the continental margin, and this increases the deflections of the continuous plate.

The flexural rigidities of the continental and oceanic lithosphere are taken to be constant because the thermal structure has negligible lateral variation for the margin ages of greatest interest. The rigidities are also equated so that we obtain a lower bound on the flexural shear stresses unless the continental rigidity is lower, which is generally not the case (Watts, Karner & Steckler 1982; Karner & Watts 1983). Thus we take

$$D_c = D_o = D(t) = \frac{E h^3(t)}{12(1 - \nu^2)}, \tag{3}$$

setting Young's modulus $E = 10^{11}$ Pa and Poisson's ratio $\nu = 0.25$. For the elastic thickness $h(t)$, we use the depth at time $t$, the margin age, to plate-model isotherms beneath which stresses are assumed to relax on long time-scales. This approach is similar to that used by Sandwell & Schubert (1982) and Sandwell (1984) for fracture zones, except that temperature boundary conditions at a fracture zone are well defined, in contrast with a continental rift, and thus they were able to take lateral variations in temperature and flexural rigidity into account. We define the elastic layer by the isotherms $T_r = 400°$, 600°, and 800 °C at the margin. The lower end of this range is defined by seamount loading (e.g. Watts 1978; Calmant, Francheteau & Cazenave 1990; Wessel 1992), intermediate values are derived from flexure at fracture zones (Parmentier & Haxby 1986; Wessel & Haxby 1990), and high values are obtained from yield-adjusted studies of subduction zones (McNutt 1984; McAdoo, Martin & Poulouse 1985) and intraplate seismicity (Wiens & Stein 1985). The higher values are more likely applicable to thermally undisturbed lithosphere. Stein & Stein (1992) have inverted the most complete data set for the plate-model thermal parameters, obtaining a best fit with a plate thickness of 95 km and a basal temperature maintained at 1450 °C; using their results, the chosen isotherms define brittle/elastic layer thicknesses of 26, 39, and 52 km for old lithosphere, with time variations as shown in Fig. 3.

At any given time, the flexural response of the oceanic lithosphere is the solution to eq. (2) that is matched at $x = 0$ to that of eq. (1):

$$w(x, t) = \exp[-x/\lambda_o(t)] \times \left[ c_1(t) \cos\frac{x}{\lambda_o(t)} + c_2(t) \sin\frac{x}{\lambda_o(t)} \right], \qquad x \geq 0, \tag{4}$$

**Table 1.** Symbols.

| Symbol | Definition | Units (and value if fixed) |
|---|---|---|
| $A$ | pre-exponential constant | $s^{-1}$ |
| $b$ | length of olivine Burgers vector | 0.5 nm |
| $d$ | grain size | 1 cm |
| | lithospheric thickness | m |
| $D$ | flexural rigidity | N m |
| $D_c D_o$ | continental, oceanic rigidities | N m |
| $E$ | Young's modulus | $10^{11}$ Pa |
| $E^*$ | activation energy | J $mol^{-1}$ |
| $f$ | failure function | N $m^{-1}$ |
| $F$ | mean degree of melting | |
| $F_r$ | integrated frictional resistance | N $m^{-1}$ |
| $g$ | gravitational acceleration | 9.8 m $s^{-2}$ |
| $G$ | shear modulus | 80 GPa |
| $h$ | brittle/elastic layer thickness | m |
| | height of gravity current | m |
| $h_0$ | hydrostatic head for gravity current | m |
| $H$ | depth of mantle shear flow | m |
| $l$ | width of rift conduit | m |
| $L$ | width of non-subducting plate | m |
| $m$ | grain-size exponent | |
| $n$ | stress exponent | |
| $p$ | hydrodynamic pressure | Pa |
| $p_f$ | pore fluid pressure | Pa |
| $P$ | static pressure | Pa |
| $q$ | inverse flexural parameter | $m^{-1}$ |
| $r$ | radial coordinate of corner flow | m |
| $R$ | universal gas constant | 8.3 J $mol^{-1}$ $K^{-1}$ |
| $t$ | time (margin or rift age) | s |
| $t_f$ | flood advancement time | s |
| $t_p$ | rift penetration time | s |
| $T$ | temperature | K |
| $T_m$ | mantle temperature | 1723 K |
| $T_r$ | relaxation temperature | °C |
| $T_s$ | surface temperature | 273 K |
| $v$ | velocity | m $s^{-1}$ |
| $v_r$ | rift velocity | m $s^{-1}$ |
| $v_s$ | slab sinking velocity | m $s^{-1}$ |
| $V$ | integrated flexural shear stress | N $m^{-1}$ |
| $V^*$ | activation volume | $m^3$ $mol^{-1}$ |
| $w$ | flexural deflection | m |
| $w_0$ | expected subsidence at margin | m |
| $x$ | horizontal distance seaward from margin | m |
| $x_m$ | corner flow truncation length | m |
| $x_n$ | position of gravity current's nose | m |
| $z$ | downward distance normal to plate surface | m |
| $z_m$ | mantle height in rift conduit | m |
| $\eta$ | dynamic viscosity | Pa s |
| $\eta_{diff}$ | viscosity due to diffusion creep | Pa s |
| $\eta_{disl}$ | viscosity due to dislocation creep | Pa s |
| $\theta$ | plate surface/fault angle | degrees |
| | corner flow angular coordinate | degrees |
| $\kappa$ | thermal diffusivity | $8 \times 10^{-7}$ $m^2$ $s^{-1}$ |
| $\lambda_c \lambda_o$ | continental, oceanic flexural parameters | m |
| $\mu$ | coefficient of fault friction | |
| $\nu$ | Poisson's ratio | 0.25 |
| | kinematic viscosity | $m^2$ $s^{-1}$ |
| $\xi$ | landward distance from ridge | m |
| $\xi_m$ | corner flow truncation length | m |
| $\rho_l$ | lithospheric density | kg $m^{-3}$ |
| $\rho_m$ | mantle density | 3330 kg $m^{-3}$ |
| $\rho_w$ | water density | 1000 kg $m^{-3}$ |
| $\sigma_a$ | longitudinal applied stress | Pa |
| $\sigma_n$ | normal stress on fault | Pa |
| $\sigma_r$ | stress due to ridge push | Pa |
| $\sigma_s$ | stress due to margin slope | Pa |
| $\sigma_\tau$ | stress due to basal shear | Pa |
| $\tau$ | basal shear stress | Pa |
| $\tau_a$ | shear stress resolved from $\sigma_a$ | Pa |
| $\tau_f$ | resolved flexural shear stress | Pa |
| $\tau_m$ | maximum shear stress in corner flow | Pa |
| $\tau_r$ | average frictional resistance of fault | Pa |
| $\psi$ | streamfunction | $m^2$ $s^{-1}$ |

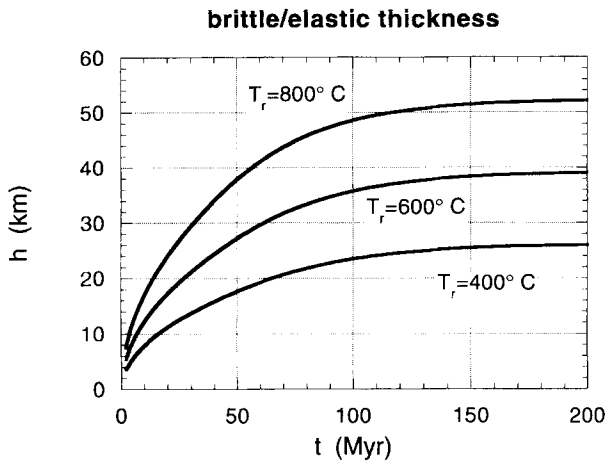


**Figure 3.** Thickness $h$ of the brittle/elastic layer versus margin age $t$ for three temperatures $T_r$ above which stresses are assumed to relax on long time-scales. Results are based on Stein & Stein's (1992) cooling-plate thermal model.

where

$$c_1(t) = \frac{w_0(t)}{1+\Lambda^2}, \qquad c_2(t) = \frac{(1-\Lambda)w_0(t)}{(1+\Lambda)(1+\Lambda^2)}, \tag{5}$$

$$\lambda_c(t) = \left[\frac{4D(t)}{\rho_m g}\right]^{1/4}, \qquad \lambda_o(t) = \left[\frac{4D(t)}{(\rho_m - \rho_w)g}\right]^{1/4}, \qquad \Lambda = \frac{\lambda_c}{\lambda_o}, \tag{6}$$

and $w_0(t)$ is the change in the sea-floor compensation depth from the ridge to the margin, i.e. the subsidence expected for sea-floor of the same age. The above may be simplified at the margin to show that, using $\rho_m = 3330$ kg $m^{-3}$ and $\rho_w = 1000$ kg $m^{-3}$ as in Stein & Stein (1992), the displacement of the oceanic lithosphere upwards from its compensation depth is $w(0, t) \approx 0.54\, w_0(t)$.

The integrated shear stress at the margin on the plane normal to the plate surface is given by

$$V(t) = D\left.\frac{d^3 w}{dx^3}\right|_{x=0} = 2D(t)\frac{c_1(t) + c_2(t)}{\lambda_o^3(t)}, \tag{7}$$

which will asymptotically approach 1.4, 2.0, and $2.4 \times 10^{12}$ N $m^{-1}$, respectively, for $T_r = 400°$, 600°, and 800 °C. Fig. 4 shows the growth in the average shear stress $V/h$.

## 2.4 Margin shear strength

Following Brace & Kohlstedt (1980), we assume that the margin has pre-existing fractures on which slip can occur. We also ignore creep in the lower lithosphere as it makes no contribution to the long-term strength. The margin strength, then, is the integrated frictional resistance of a fault cutting the brittle/elastic layer and depends on the fault length, the average normal stress on the fault plane, and on the coefficient of fault friction. (We omit cohesion at the fault surface given the large uncertainty in the friction coefficient; see below.) The length of the fault partly depends, in turn, on its orientation, as do the normal stresses resolved onto it. Taking tensile stresses to be positive, the total shear resistance provided by

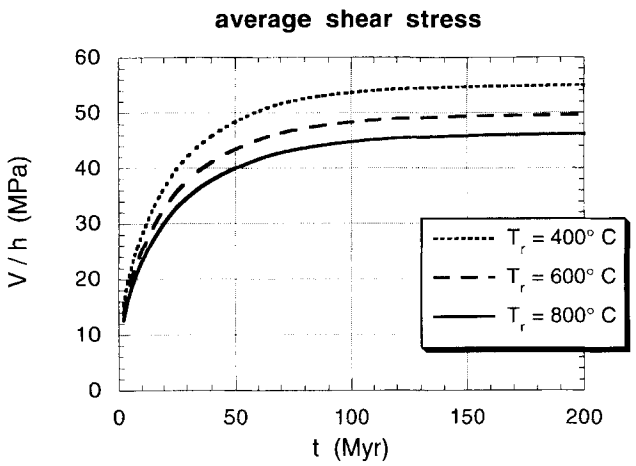


**Figure 4.** Average flexural shear stress at a passive margin on the plane normal to the plate surface.

such a fault at time (margin age) $t$ is

$$F_r(\theta, t) = \frac{-\mu}{\sin\theta}\int_0^{h(t)} [\sigma_n(z, \theta, t) + p_f]\, dz, \qquad (8)$$

where $\theta$ is the angle the fault makes with the plate surface, $\mu$ is the coefficient of friction, $\sigma_n$ is the normal stress on the fault, $p_f$ is the pore fluid pressure (assumed to be hydrostatic), and $z$ measures downward distance perpendicular to the plate surface.

Estimates of the coefficient of fault friction range from a laboratory-derived high value near 0.85 (Byerlee 1978; Brace & Kohlstedt 1980) through values near 0.5 obtained for clay-rich fault gouge (Morrow, Shi & Byerlee 1982) and fault-derived serpentinites (Dengo & Logan 1981) to values $<0.2$ inferred from stress orientations and the absence of a heat-flow anomaly near the San Andreas fault (Henyey 1968; Mount & Suppe 1987; Zoback *et al.* 1987; Lachenbruch & McGarr 1990), and simulations predicting stress orientations and the distribution of fault slip throughout California (Bird & Kong 1994). Below we will consider the consequences of friction coefficients $\mu = 0.2$, 0.5, and 0.85, recognizing that the lower end of this range may only apply if faults from the basin-forming rift event can be reactivated.

The normal stresses on the fault include lithostatic pressure and the normal components resolved from applied stresses and the flexural shear force,

$$\sigma_n(z, \theta, t) = -\bar{\rho}_l(z, t) g z + \sigma_a(t)\sin^2\theta - \frac{V(t)}{h(t)}\sin\theta\cos\theta, \qquad (9)$$

where $\bar{\rho}_l$ refers to the average lithospheric density above the depth in question and $\sigma_a$ is a longitudinal applied stress. Specifically,

$$\sigma_a(t) = \sigma_s(t) + \sigma_\tau(t) + \sigma_r(t), \qquad (10)$$

where the right-hand-side terms are stresses arising from the seaward slope of the margin, basal shear stresses, and ridge push (Fig. 5). Fibre stresses are not included in $\sigma_n$ because the elastic layer bears them on long time-scales and is rheologically homogeneous (ignoring the fault). These stresses therefore integrate to zero and make no contribution to $F_r$ (eq. 8).

Assuming that curvatures are small, as they may be shown to be from eq. (4), the tension due to the margin's slope is

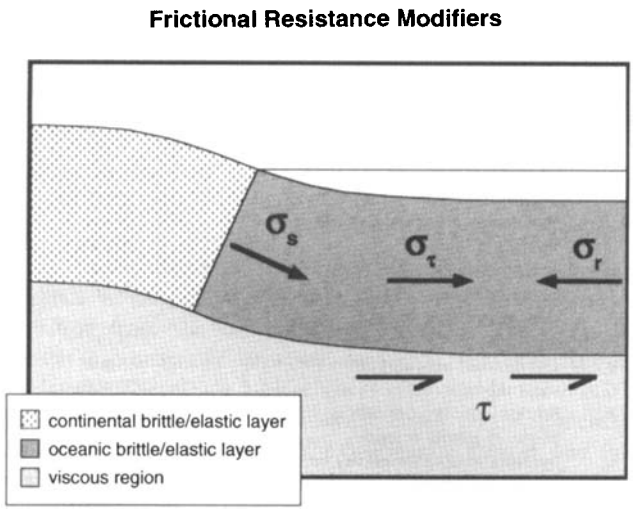


**Figure 5.** Sources of deviatoric normal stress at a passive margin. The long-term margin strength, defined by the frictional resistance of a fault, is increased by ridge push stresses $\sigma_r$ transmitted through the brittle/elastic layer, but decreased by stresses $\sigma_\tau$ supporting ridge-directed basal tractions $\tau$, and by $\sigma_s$, the component of the layer's weight directed down the slope of the flexural profile.

simply the integrated downdip component of the plate's weight,

$$\sigma_s(t) = \bar{\rho}_l(h, t) g w(0, t). \qquad (11)$$

For the parameters given above, the displacement at the margin from the compensation depth grows to 1.66 km. The asymptotic values of $\bar{\rho}_l$ vary with $T_r$ by only 0.6 per cent, so this stress reaches 56 MPa, regardless of the value of $T_r$ (see Fig. 6).

The force associated with ridge push (e.g. Parsons & Richter 1980) must be supported by the brittle/elastic layer over long time periods, giving

$$\sigma_r(t) = -\frac{g}{2h(t)}(\rho_m - \rho_w) w_0^2(t) - \frac{g}{h(t)}\int_0^{95\,\mathrm{km}} [\rho_l(z, t) - \rho_m] z\, dz, \qquad (12)$$

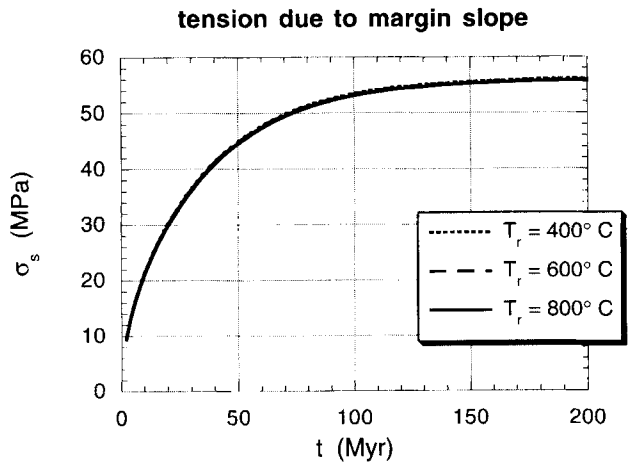


**Figure 6.** Contribution to margin-normal deviatoric tension due to the slope of the flexural profile. Values are essentially independent of $T_r$ because the average densities are nearly identical.

where the brittle/elastic thickness $h$ is evaluated at the margin. As shown in Fig. 7, this stress asymptotically approaches $-88$, $-59$, and $-44$ MPa, respectively, for $T_r = 400°$, $600°$, and $800\,°C$. Note that for old margins with $T_r = 600°$, $\sigma_s$ and $\sigma_r$ approximately balance (Fig. 8). When the ridge push is distributed over the thick layer defined by the $800\,°C$ isotherm, the tension due to the margin slope more than offsets it after 40 Myr.

The final, and most problematic, contributor to the normal stress on the margin is due to the shear stress $\tau$ coupling the plate and underlying mantle. The stress $\sigma_\tau$ is simply defined by

$$\sigma_\tau(t) = \frac{1}{h(t)} \int_0^{vt} \tau(x, t)\, dx, \tag{13}$$

where $v$ is the half-spreading rate; the difficulty lies in reasonably defining $\tau(x, t)$.

An important point here is that it is possible for the plate to experience ridge-directed basal shear ($\tau > 0$) under the oceanic lithosphere and mid-plate tension for the plate geometry depicted in Fig. 2(a). To show this, we consider the system from a purely kinematic standpoint, assuming the non-subducting plate is at rest and bounded on the right by a ridge. If the ridge spreads symmetrically and migrates to the right at velocity $v$, and the left-bounding subducting slab sinks vertically with velocity $v_s$, then the ridge creates a clockwise circulation (with $\tau > 0$) while the subducting slab creates a counterclockwise circulation ($\tau < 0$). An analytical, generalized corner-flow solution developed in the Appendix explicitly demonstrates that this flow allows a tensile state of stress within the non-subducting plate despite compressive bounding stresses at the trench and near the ridge,

$$\sigma(\xi) = \sigma_r + \frac{4\eta v}{\pi h(\xi)} + \frac{\eta}{h(\xi)} \times \left\{ \frac{4v}{\pi} \left[ \ln\left(\frac{\xi}{\xi_m}\right) - \frac{2\xi}{L} + \frac{\xi^2}{2L^2} \right] - \frac{8v_s}{(\pi^2 - 4)} \ln\left[\frac{L}{(L-\xi)}\right] \right\} \tag{14}$$

for $\xi > \xi_m$, where $\xi$ represents horizontal distance landwards from the ridge, $\xi_m$ is the cutoff to the corner flow imposed to avoid divergent stresses near the origin (see Appendix), and $\eta$ is a uniform dynamic viscosity. As the distance $L$ between the ridge and trench increases with time but $\xi_m$ remains fixed, this model predicts a (weak) trend towards more tensile stresses at intermediate $\xi$ with time (Fig. 9), as required by our model. Unfortunately, further use of this model would force us to define a second plate velocity $v_s$, the manner in which the corner-flow singularities are avoided (i.e. $\xi_m$), and, most problematically, the width of the continent. As our goal is to provide a preliminary examination of our model's prospects, we instead adopt two simple models of the flow beneath the oceanic lithosphere, recognizing that in reality, the flow will be significantly more complex and require careful modelling.

Our models for the basal shear stress are based on a simple shear flow driven by the surface plate. This is intended to mimic the region far from a subduction zone that is primarily driven by coupling to the coherent surface layer. We use the

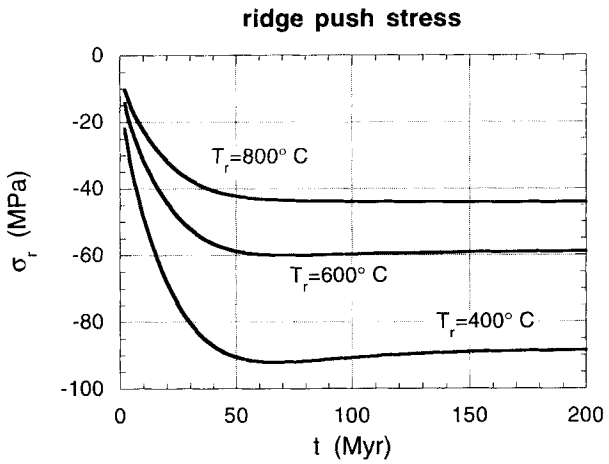


**Figure 7.** Ridge push force at the margin divided by the thickness of the brittle/elastic layer that must support it on long time-scales.

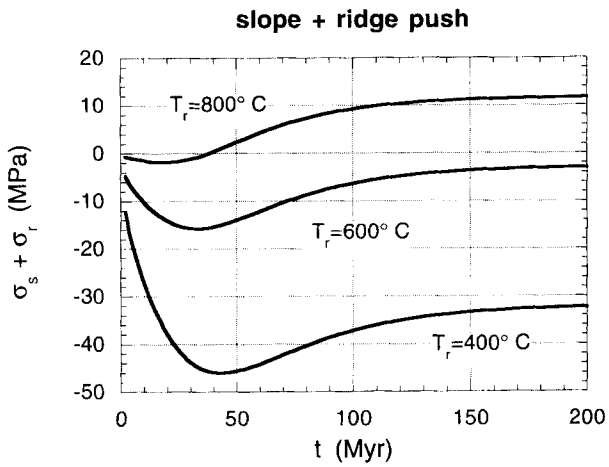


**Figure 8.** Balance between margin-normal stresses due to the margin's slope and ridge push. The elastic layer thickness does not affect $\sigma_s$, but redistributes the ridge push. For large $h$, therefore, $\sigma_s$ can more than offset $\sigma_r$.

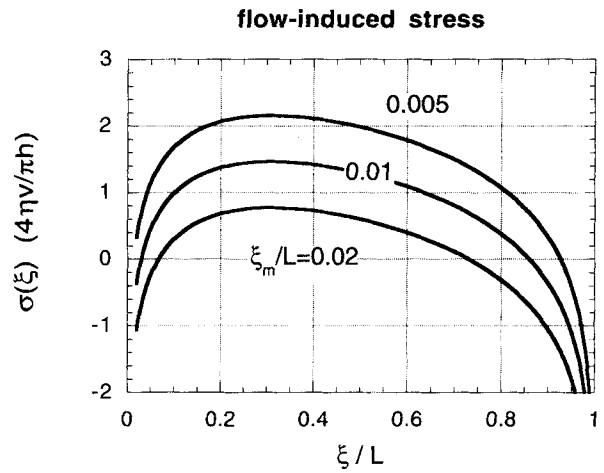


**Figure 9.** Stress induced by ridge push and the generalized corner flow. The vertical axis measures stress, with tension positive, in units of $4\eta v/\pi h$. The horizontal axis measures distance from the ridge in units of $L$, so that the trench lies at the right at $\xi = L$. For demonstration, these curves arbitrarily assume $\sigma_r = -2$, and that $v = v_s$. As the plate length $L$ increases with time but the corner-flow cutoff $\xi_m$ does not, decreasing $\xi_m/L$ corresponds to increasing plate age.

fact that the shear stress $\tau = \eta\, dv_x/dz$ is independent of depth in a shear flow, and we take the integrated velocity gradient to be the surface velocity $v$. This gives

$$\tau(x,t) = v\left[\int_0^H \frac{dz}{\eta(x,z,t)}\right]^{-1}, \qquad (15)$$

where $H$ is the flow's depth. This model underestimates the shear in the neighbourhood of the ridge, where the upward flow required by surface divergence means that horizontal velocities decrease more rapidly with depth.

Our first application of eq. (15) uses published models of radially averaged viscosity to obtain fixed values of the shear stress. The simplest possible such model would use a constant viscosity $\eta = 10^{21}$ Pa s (e.g. Haskell 1935, 1936; Cathles 1975; Peltier 1989) in a shear flow filling the upper mantle. With reasonable plate velocities of 1–3 nm s$^{-1}$ (1 nm s$^{-1}$ $\approx$ 32 mm yr$^{-1}$), and setting $H = 570$ km, this approach gives $1.8 < \tau < 5.3$ MPa.

To compare this value with other results, we focus on the bracketed term in eq. (15), which has a value of $1.8 \times 10^{15}$ Pa s m$^{-1}$ for the above model. Hager (1991) compiled a number of recent viscosity estimates based on the response to Pleistocene deglaciation that give $1.6 \times 10^{14}$–$1.8 \times 10^{15}$ Pa s m$^{-1}$ in contrast with his own model, based on the geoid, plate-driving forces, and advected heat flux, that gives $6.5 \times 10^{13}$ Pa s m$^{-1}$. This estimate, like those given below, has the virtue of being based on the density anomalies responsible for convection and responses at convective time-scales. Hager discussed several sources of uncertainty, however, including limited resolution of tomographic models, a lack of azimuthal variation in the rheology, particularly in the lithosphere, and the high sensitivity of the geoid kernels' amplitude to the viscosity structure itself. Forte, Peltier & Dziewonski (1991) used tomographic data and plate velocities (horizontal surface divergence) to formally invert for the viscosity structure, accounting for data uncertainties and model resolution. Trade-offs in viscosity between layers allow the best-fitting model to have a weaker lithosphere than asthenosphere, but a model that fits almost as well reverses this and gives $1.5 \times 10^{15}$ Pa s m$^{-1}$ for $v$'s coefficient in eq. (15). King & Masters (1992) inverted three different shear velocity models and the geoid, resulting in an average of $1.9 \times 10^{14}$ Pa s m$^{-1}$ over the upper mantle and the interesting feature that the minimum viscosity in each case was in the 400–670 km layer. Forte, Dziewonski & Woodward (1993) found that the geoid, plate motions, and core–mantle boundary topography are all well fit using a model with $\eta = 10^{21}$ Pa s throughout the upper mantle, except for an exponential drop by two orders of magnitude over the bottom 70 km. This model was inspired by the correlation between heterogeneity in shear velocity gradients at those depths and the geoid, and gives $5.0 \times 10^{14}$ Pa s m$^{-1}$. A value of $3 \times 10^{14}$ Pa s m$^{-1}$ would appear justified by these results giving, for $v = 1$, 3 nm s$^{-1}$, $0.3 < \tau < 0.9$ MPa. In what follows, therefore, one definition of the basal shear tractions will be the fixed values $\tau(x,t) =$ 0.5, 1.0 MPa.

Forsyth & Uyeda (1975) and Chapple & Tullis (1977) both argued, based on inversions, that the dominant forces acting on plates arise from the buoyancy of slabs and resistive tractions applied to slab surfaces or at trenches; other forces were found to be secondary. This has been widely interpreted to mean that basal tractions are inconsequential. By calibrating with ridge push, however, Forsyth & Uyeda estimated that the mean basal drag stress acting on a plate is 0.5 MPa (for a plate moving at 80 mm yr$^{-1}$), which is one of our fixed values. The mean taken between the ridge and passive margin can be larger if, as in our model, the shear stress changes sign beneath the plate. Furthermore, because the role of basal drag is secondary in the plate's force balance, it is associated with a small eigenvalue in these inversions. A factor of two to obtain our other fixed basal stress would therefore appear compatible with this work.

These studies suffer from a number of shortcomings and must be used with caution in any case. The basic problem is that there are few oceanic plates and they do not experience the same controls on their behaviour. The Indian and Australian plates, for example, are the only ones that have significant fractions of both continental area and subducting margin, yet one also experiences continental collision. Of the four major subducting oceanic plates—the Cocos, Philippine, Nazca and Pacific—the plate ages at the trench are variable around and among the plates ($\sim$15–25, 20–50, 15–80, and 45–155 Myr, respectively; Jarrard 1986), the absolute trench lengths vary considerably, and, while there is modest variation in the fraction of the boundary that subducts, the areas differ dramatically, and thus the ratios of trench length to basal area do also. Finally, the Nazca plate has two regions of low-angle subduction beneath South America (e.g. Isacks & Barazangi 1977) that make its force balance unique among modern oceanic plates. These variations make it dangerous to invert for the relative importance of each control from so few observations, i.e. plates. These studies also did not use plate age to infer buoyancy variations, and significant changes have been made in estimates of plate velocities: Forsyth & Uyeda (1975) took the Nazca and Cocos plates to have average velocities $\sim$5 per cent smaller and greater, respectively, than the Pacific plate, while Gripp & Gordon (1990) estimated that they are roughly 55 per cent and 40 per cent slower. In short, the magnitude and role of basal tractions must be considered poorly known, but our fixed values are at least reasonable estimates.

Our second approach to defining $\tau(x,t)$ also uses a simple shear flow, but includes an attempt to account for the upper mantle's rheological behaviour by using a temperature- and depth-dependent viscosity in eq. (15). We take the geobaric gradient to be constant and take the temperature from a half-space cooling model: the plate model used elsewhere in this paper does not define temperatures below the boundary layer, so we use

$$T(x,z,t) = T_s + (T_m - T_s)\,\mathrm{erf}\left[\frac{z}{2\sqrt{\kappa(t - x/v)}}\right], \qquad (16)$$

recalling that $t$ refers to the age of the margin. We set $T_s = 273$ K and use Stein & Stein's (1992) mantle temperature $T_m = 1723$ K and thermal diffusivity $\kappa = 8 \times 10^{-7}$ m$^2$ s$^{-1}$. Most estimates of the mantle's potential temperature are significantly lower, such as McKenzie & Bickle's (1988) value of 1553 K, and thus the mantle in our model is relatively weak.

To further avoid overestimating the viscosity, we follow Karato & Wu (1993) who emphasize that either dislocation or diffusion creep can locally dominate, depending on the

temperature, pressure, and shear stress. Thus,

$$\eta(x, z, t) = \min(\eta_{\text{disl}}, \eta_{\text{diff}}), \tag{17}$$

where

$$\eta_{\text{disl}} = \frac{G^n}{A}\tau^{1-n}\exp\left(\frac{E^* + PV^*}{RT}\right), \tag{18}$$

and

$$\eta_{\text{diff}} = \frac{G}{A}\left(\frac{d}{b}\right)^m \exp\left(\frac{E^* + PV^*}{RT}\right). \tag{19}$$

Here, $G$ is the shear modulus, $d$ is the grain size, $b$ is the length of the olivine Burgers vector, $P$ is the pressure, and $R$ is the gas constant. The stress and grain size exponents $n$ and $m$ take different values for 'dry' (water-absent) and 'wet' (water-saturated) conditions, and the pre-exponential constants $A$, activation energies $E^*$, and activation volumes $V^*$ differ both with volatile content and between the two creep mechanisms. The activation volumes for dislocation creep are quite uncertain, but we take values from the middle of the reported ranges: $V^* = 20\ \text{cm}^3\ \text{mol}^{-1}$ for dry conditions and $V^* = 15\ \text{cm}^3\ \text{mol}^{-1}$ for wet. We use a fixed grain size of 1 cm (Karato & Spetzler 1990) and the remaining parameters as given by Karato & Wu (1993).

Because dislocation creep depends on the shear stress, eq. (15) must be solved iteratively, yielding results as shown in Fig. 10. For a wet mantle, the average shear stress $\bar{\tau}$ on the base of the plate reaches 0.5 MPa in ~375, 310, or 270 Myr for $v = 1$, 2, or 3 nm s$^{-1}$. For a dry mantle, $\bar{\tau} = 1$ MPa after ~115, 85, or 75 Myr. Note that at 200 Myr, the shear stress exerted on a fast-moving plate by a dry mantle is 6.5 times larger than for a wet mantle. Karato & Wu (1993) used data from basalts and electrical conductivities to argue that the mantle is saturated beneath volcanic arcs and undersaturated elsewhere, but it is unfortunate that our model is so strongly dependent on this poorly known attribute of the mantle.

The normal stresses $\sigma_\tau$ corresponding to the predicted $\tau(x, t)$ are shown in Fig. 11 for both the fixed values and for the wet and dry shear flows with half-space cooling. Except where

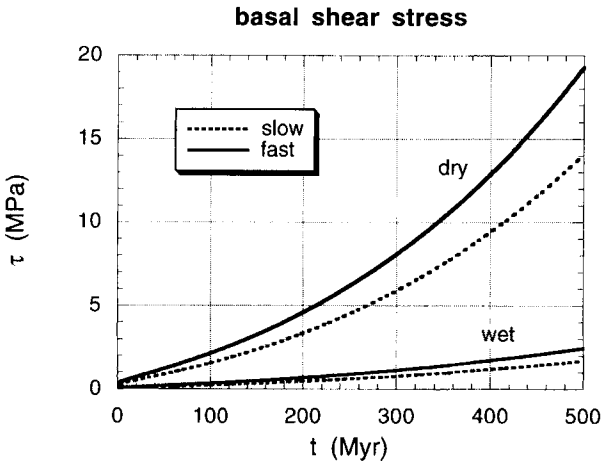


**Figure 10.** Basal shear stress resulting from plate-driven shear flows that fill the upper mantle. A temperature- and pressure-dependent rheology and half-space cooling are assumed. See text for details. 'Slow' and 'fast' denote plate speeds and half-spreading rates of 1 and 3 nm s$^{-1}$ (32 and 95 mm yr$^{-1}$). At 200 Myr, the shear stress exerted on a fast moving plate by a 'dry' mantle is 6.5 times larger than for a 'wet' mantle. For a wet mantle, the average shear stress $\tau$ on the base of the plate reaches 0.5 MPa in ~375, 310, or 270 Myr for $v = 1$, 2, 3 nm s$^{-1}$. For a dry mantle, $\bar{\tau} = 1$ MPa after ~115, 85, or 75 Myr.

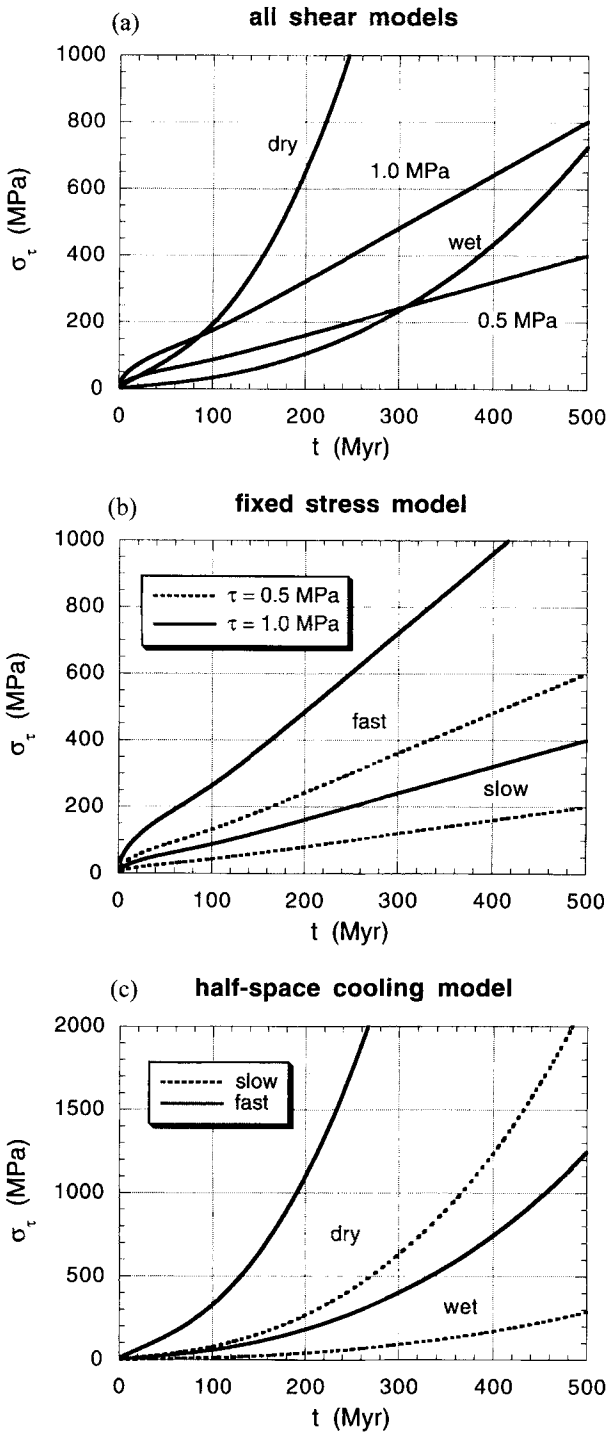


**Figure 11.** Margin-normal deviatoric tension due to basal shear tractions. (a) A comparison of fixed stress and cooling half-space shear flow models using $T_r = 600\,^\circ\text{C}$ and $v = 2$ nm s$^{-1}$ (63 mm yr$^{-1}$). (b) Comparison of fixed stress models for slow and fast (1 and 3 nm s$^{-1}$) growing plates. (c) Comparison of wet and dry plate-driven shear flows with half-space cooling.

otherwise noted, all examples use $T_r = 600\,^{\circ}\mathrm{C}$ and $v = 2\ \mathrm{nm\ s^{-1}}$ ($63\ \mathrm{mm\ yr^{-1}}$); we caution that this half-spreading rate adds a hemisphere of oceanic lithosphere to the plate in $\sim 300$ Myr.

The total applied stress $\sigma_a$ acting normal to the margin due to its slope (eq. 11), ridge push (eq. 12), and basal shear tractions (eq. 13) is shown in Fig. 12 for the fixed-value and the wet and dry basal shear models. Note that some models have a period in which ridge push dominates over other contributors so that the applied stress complements, rather than offsets, the lithostatic pressure. In all cases, however, the tension due to inhibited subsidence and basal shear tractions dominates at greater ages. With this description of $\sigma_a$, we have now defined all of the contributors to the normal stress $\sigma_n$ (eq. 9), which in turn enters the definition of the integrated fault friction $F_r$ (eq. 8).

### 2.5 Margin failure

This model predicts that the oceanic and continental lithosphere will decouple when a fault can slip at their interface. For this, the integrated frictional resistance offered by some plane must be exceeded by the integrated shear stress applied to it. This shear stress has two components. One,

$$\tau_a(\theta, t) = \sigma_a(t) \sin\theta \cos\theta, \tag{20}$$

is the shear stress resolved onto the plane from the longitudinal applied stress $\sigma_a$ (eq. 10) when the plane makes an angle $\theta$ with the plate surface (dipping seawards). The other,

$$\tau_f(\theta, t) = \frac{V(t)}{h(t)} \sin^2\theta, \tag{21}$$

is the component of the flexural shear stress (eq. 7) resolved onto this plane. The proximity to failure can therefore be described by

$$\begin{aligned} f(\theta, t) &= F_r(\theta, t) - \frac{h(t)}{\sin\theta}[\tau_a(\theta, t) + \tau_f(\theta, t)] \\ &= \frac{\mu(\bar{\rho}_l - \rho_w)gh^2}{2\sin\theta} - h\sigma_a(\mu\sin\theta + \cos\theta) \\ &\quad + V(\mu\cos\theta - \sin\theta), \end{aligned} \tag{22}$$

and failure occurs when there is a plane on which $f = 0$. The 'fault' is the plane that gives the minimum of $f$ with respect to $\theta$. It must be located numerically prior to failure, but at failure we have both $f = 0$ and $\partial f/\partial\theta = 0$, giving

$$\cot\theta = \pm\sqrt{1 - \frac{2(\mu h\sigma_a + V)}{\mu(\bar{\rho}_l - \rho_w)gh^2}}. \tag{23}$$

The positive root corresponds to tensile failure.

Having defined the fault orientation through time, we can

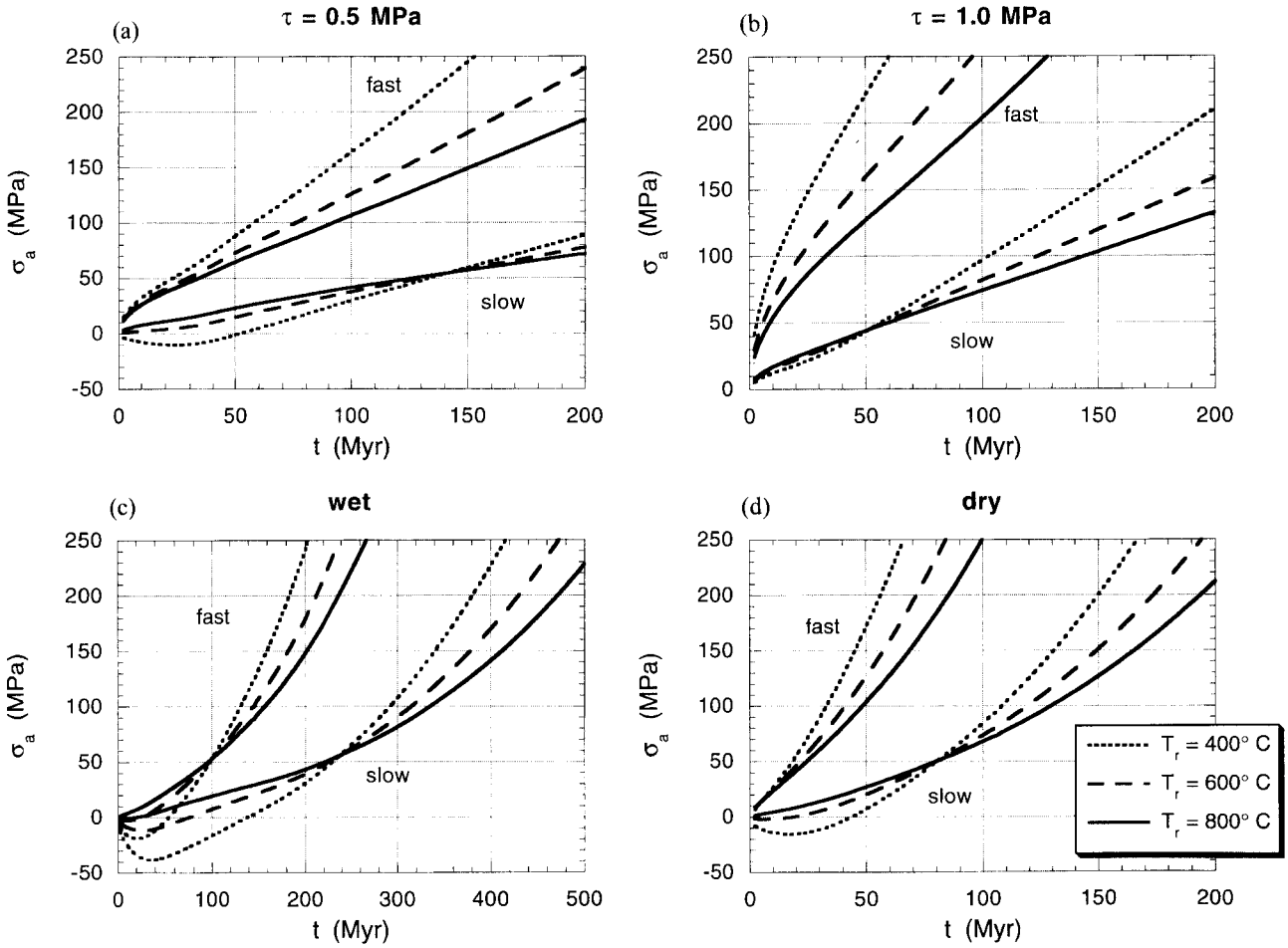


**Figure 12.** Total margin-normal deviatoric tension due to the margin slope, basal shear tractions, and ridge push. 'Slow' and 'fast' denote plate speeds and half-spreading rates of 1 and 3 nm s$^{-1}$. Panels show results for four different basal shear models, as labelled.

now consider the average frictional resistance it offers,

$$\tau_r(\theta, t) = F_r(\theta, t)\frac{\sin\theta}{h(t)}, \qquad (24)$$

which is shown in Fig. 13 for several parameter combinations, but using $\mu = 0.5$, $T_r = 600\,^{\circ}\mathrm{C}$, and $v = 2$ nm s$^{-1}$, except where otherwise noted. The curves are truncated at the time the margin fails. Fig. 13(a) shows the variations among basal shear models. The strength of the margin grows with the average lithostatic pressure in the brittle layer and with ridge push for $\sim 100$ Myr, although there is considerable variability in the age at which the strength peaks (e.g. Fig. 13d). After quantities related to plate cooling saturate, the strength decays with the continued growth of integrated basal tractions. Fig. 13(b) illustrates the scaling of strength with the friction coefficient. The curves for different $\mu$ converge towards the point at which the margin's long-term shear strength vanishes. That occurs when the pore fluid pressure and the fault-normal component of the applied stress balance lithostatic pressure and the normal component of the flexural shear stress (eqs 8 and 9). The age at which this occurs depends strongly, however, on the temperature above which stresses relax, as shown in Fig. 13(c) for the basal shear model that is weakest at large ages. The increase with $T_r$ is due to both the greater average lithostatic pressure and the thicker layer over which basal tractions are balanced. Finally, Fig. 13(d) illustrates the dependence of strengths on plate velocity through both the surface area over which shear stresses are applied (eq. 13) and the shear strain rates inferred for the underlying mantle (eq. 15).

To examine the conditions under which margins fail, we used the basal shear models described above ($\tau = 0.5$, 1.0 MPa and half-space cooling of a wet or dry upper mantle) and varied the relaxation isotherm ($T_r = 400°$, 600°, 800 °C), friction coefficient ($\mu = 0.2$, 0.5, 0.85), and the plate velocity ($v = 1$, 2, 3 nm s$^{-1}$) to obtain a suite of 108 models. These were evaluated every 2 Myr for 500 Myr. One expects from the model formulation that failure will be promoted by large basal shear stresses, a low relaxation temperature, and hence a thin brittle/elastic layer and low static pressures, a low friction coefficient, and a high plate velocity, which gives a large surface area onto which basal tractions are applied, and high strain rates in the underlying mantle (for the half-space cooling models).

Fig. 14 illustrates this behaviour and the way failure is approached in several cases. It is analogous to Fig. 13, but shows the difference between the average frictional resistance offered by the fault and the shear stresses applied to it. Failure, then, occurs when the curves go to zero. Unfortunately, widely varied times to failure are predicted from different basal shear models (Fig. 14a), and these tractions are quite uncertain. More modest variations arise from the most reasonable friction

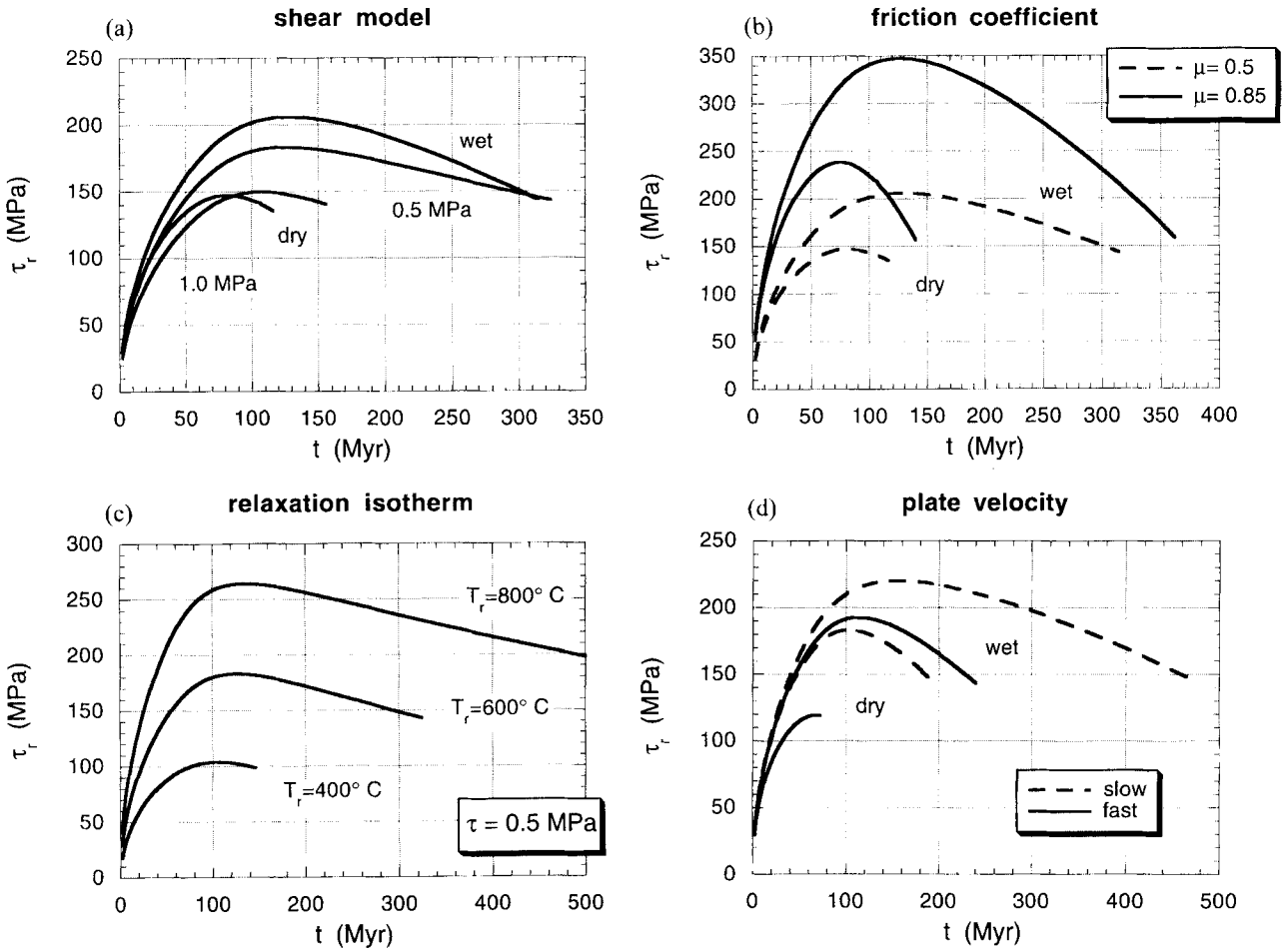


**Figure 13.** Average frictional resistance offered by a high-angle fault at the margin. Curves are truncated at the time of margin failure. Unless otherwise indicated, $\mu = 0.5$, $T_r = 600\,^{\circ}\mathrm{C}$, and $v = 2$ nm s$^{-1}$.

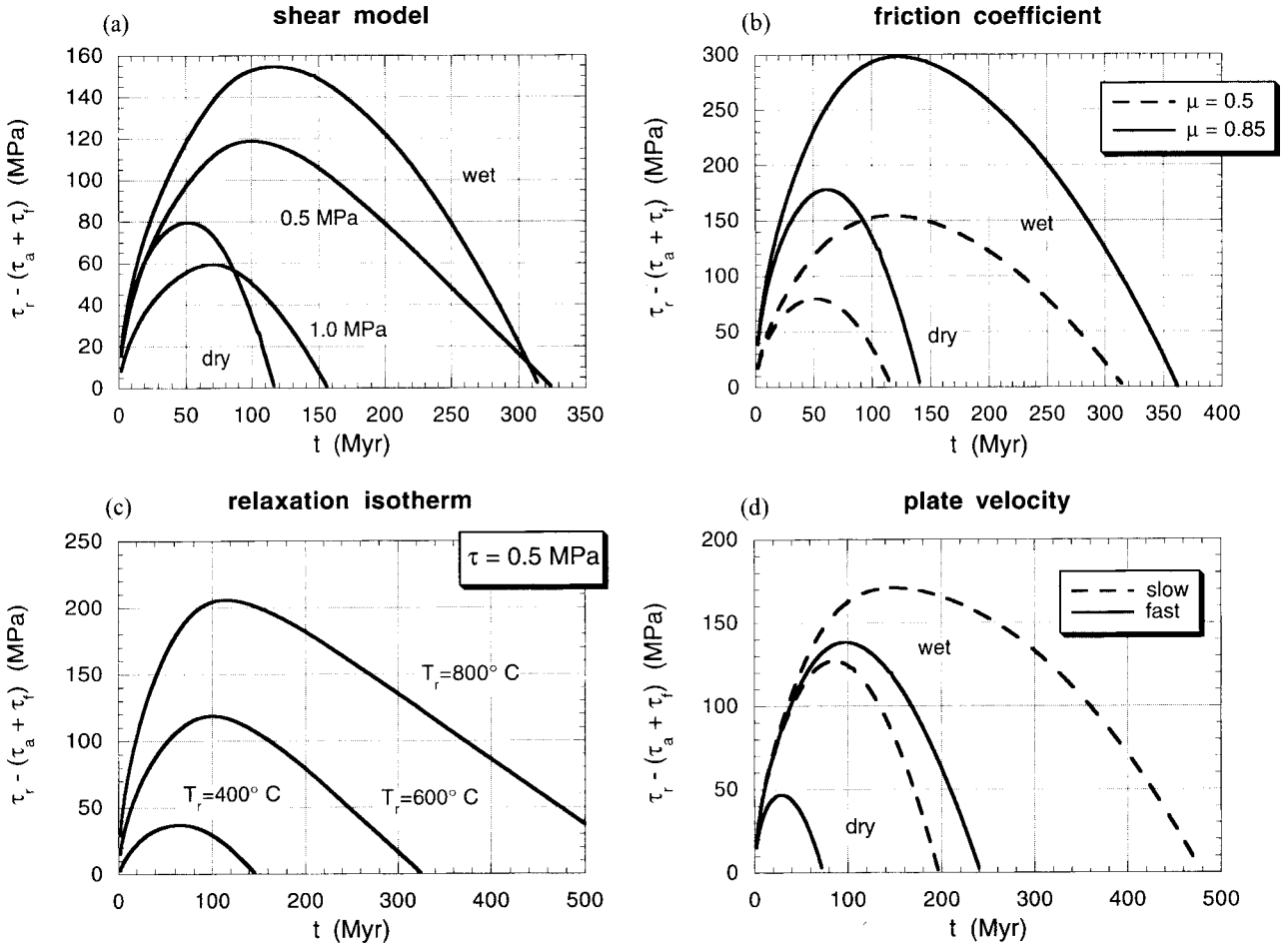


**Figure 14.** Difference between the average shear strength of the margin and the average shear stress applied to it. Shear stresses arise from normal stresses resolved onto the fault and flexure. The oceanic and continental lithosphere will decouple when these curves go to zero. Unless otherwise indicated, $\mu = 0.5$, $T_r = 600\,^{\circ}\mathrm{C}$, and $v = 2$ nm s$^{-1}$.

coefficients (Fig. 14b), but these can also be of several tens of millions of years. Indeed, any of the parameters is capable of causing large variations in the time to margin failure.

From the entire suite of models, 30 met the failure criterion $f = 0$ (eq. 22) when first evaluated at 2 Myr. Of these, 10 failed in compression. In another 13 cases, the margin did not fail within 500 Myr, while in the remaining 65 the margin failed at intermediate times. Notably, each parameter value appears in all three sets of failure times with two exceptions: no dry model lasted 300 Myr, and no model with $T_r = 400\,^{\circ}\mathrm{C}$ lasted 420 Myr. Thus, none of the parameter values is incompatible with margin failure at intermediate ages.

Models that fail immediately raise the possibility that margins are not, in fact, mechanically coupled from an early age and that flexural stresses cannot accumulate. As discussed above, however, gravity data at passive margins suggest that they are capable of supporting flexure. Large age-offset fracture zones also exhibit flexural profiles that indicate that the lithosphere maintains mechanical continuity there in spite of rapid cooling on their younger side (Sandwell & Schubert 1982; Sandwell 1984). Here we note that all but four of the 30 models that fail immediately use $\mu = 0.2$, and the other four have $T_r = 400\,^{\circ}\mathrm{C}$. Both values may well be too low. Only two models fail immediately with $T_r = 800\,^{\circ}\mathrm{C}$, and these have $\mu = 0.2$, the higher plate speeds, and a fixed basal shear stress $\tau = 1.0$ MPa, an average that even a fast plate moving over a dry mantle takes almost 75 Myr to develop.

The 13 models in which the margin did not fail have the lowest plate speed and/or the smallest basal shear stress, parameters that reduce the applied tension, rather than define inherent properties of margins. They also have more than one parameter value that promotes stability. Again, none uses the dry basal shear model, and the only two with $\tau = 1.0$ MPa have $T_r = 800\,^{\circ}\mathrm{C}$ and the lowest speed. None has the thinnest brittle/elastic layer, and the only three with $T_r = 600\,^{\circ}\mathrm{C}$ use the weaker two basal tractions and also use the lowest plate speed.

In the remaining 65 models, a variety of reasonable parameter combinations lead to margin failure in geologically plausible times. Interestingly, after avoiding immediate failure, only two more models fail within 50 Myr (both with fast plates moving over a dry mantle), which reflects the rapid growth at young margins of the brittle/elastic layer and the static pressures within it (Fig. 13). Four models fail within 300 Myr, even when we exclude the thinnest elastic layer and lowest friction coefficient and we consider only the weaker models of basal coupling (the wet model and $\tau = 0.5$ MPa). Another 19 do so with stronger coupling. An intermediate model, with $\tau = 1.0$ MPa, $T_r = 600\,^{\circ}\mathrm{C}$, $\mu = 0.5$, and $v = 2$ nm s$^{-1}$, fails uncomfortably early at 158 Myr.

As to the stress state when the margins fail, we find that

flexure contributes 19–70 per cent of the shear stress required for slip in the models that fail at intermediate times, with a median value of 29 per cent. The applied tension is necessary both to reduce the fault's strength and to apply a shear traction, but flexural shear stresses hasten failure at the margin. These shear stresses $\tau_f$ are 30–50 MPa at failure, and the applied stresses $\sigma_a$ range from 56–475 MPa, with a median value of 255 MPa. Passive margin flexure plays a significant role here as well by contributing over 50 MPa to the applied stress through $\sigma_s$. Flexure slightly steepens the faults, which make a median angle $\theta = 68°$, with some as steep as 75°.

### 2.6 Foundering

Once the conditions for tensile failure are satisfied, a rift begins to develop. Lithospheric failure cannot occur without trench-directed forces applied to the continent, and decreased coupling at the margin means that these must be increasingly balanced over the continent's smaller surface area. The continent, therefore, must move more rapidly to generate the necessary balancing tractions. The change in forces on the oceanic plate will cause motion towards the ridge in a reference frame fixed to the incipient rift. The evolution of the fault or sequence of faults that form this rift is beyond our present scope, however, partly because it is complicated by the pre-existing flexure. We will therefore take the rift to be a single, vertical conduit to allow a preliminary evaluation of the old oceanic lithosphere's potential for foundering. The non-vertical nature of the conduit affects the estimate of flooding time-scales by a factor of two or less, which is smaller than other uncertainties in the calculation. Note also that we ignored viscous resistance in assessing the likelihood of margin failure. During rifting, viscous resistance controls the rate of extension and, therefore, the displacement of isotherms.

Since the underlying mantle is hotter and less dense than the lithosphere, it will tend to rise through the rift conduit to a height of 3 km or more above the old sea-floor, i.e. to a relative height comparable to that of mid-ocean ridges. This is the situation discussed by Turcotte *et al.* (1977). It differs from a mid-ocean ridge only in that the mantle upwelling is confined to a conduit whose width is initially small. Schubert & Garfunkel (1984) have analysed the filling of such a conduit in the context of leaky transforms, and we take a similar approach. If the width of the conduit is $l(t)$ and the lithospheric thickness is $d$, the mean flow in the conduit at time $t$ is $v(z, t)$, given by

$$v(z, t) = -\frac{l^2(t)}{12\eta}\frac{\partial p}{\partial z}, \tag{25}$$

where $p$ is the hydrodynamic pressure, $z < d$ is the height at a point in the flow above the base of the lithosphere, and the mantle viscosity is $\eta$ (assumed constant). The situation is illustrated in Fig. 15. We also have the continuity requirement,

$$l(t)\frac{\partial v(z, t)}{\partial z} = -\frac{dl(t)}{dt}. \tag{26}$$

For an assumed steady rifting at velocity $v_r$, $l(t) = v_r t$, so the solution to this equation is

$$v(z, t) = \frac{dz_m(t)}{dt} + \frac{z_m(t) - z}{t}, \tag{27}$$

where $z_m(t)$ is the top of the flow. The non-zero flow at $z = 0$ is accommodated by a negligibly small pressure drop between deeper mantle and the base of the rift. There is accordingly an integral constraint for the hydrodynamic pressure drop between the base of the lithosphere and the top of the conduit flow,

$$\int_0^{z_m(t)} -\frac{\partial p}{\partial z}\, dz = g[\rho_l d - \rho_m z_m(t)], \tag{28}$$

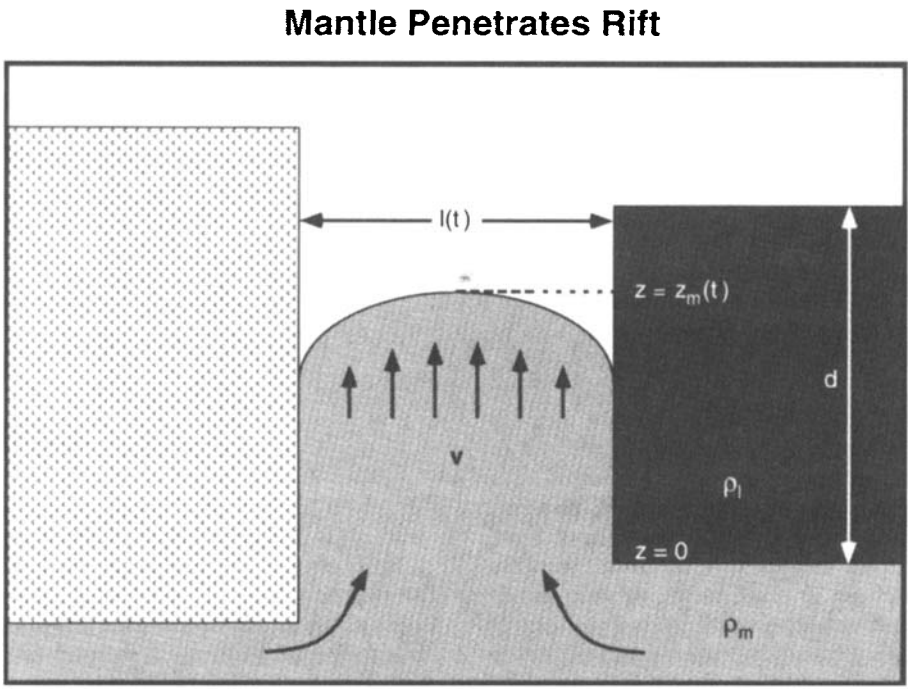


**Figure 15.** Mantle penetration of the rift between the continental and old oceanic lithosphere. Hot mantle rises with mean velocity $v$ into a conduit of width $l(t)$. The column's height above the base of the lithosphere is $z_m(t)$, and $d$ is the lithospheric thickness.

where $\rho_l$ and $\rho_m$ are mean lithospheric and mantle densities, respectively. In this and all modelling reported here, the density of overlying water is ignored; it has only a small effect on results that are only intended as rough approximations. It follows, then, that $z_m(t)$ is the solution to

$$t\frac{d}{dt}z_m^2(t) + z_m^2(t) = z_{m_0}^2(t)\left[1 - \frac{\rho_m z_m(t)}{\rho_l d}\right], \tag{29}$$

where

$$z_{m_0}(t) = \sqrt{\frac{\rho_l g d^2}{6\eta v_r}}(v_r t)\sqrt{\frac{v_r t}{d}}. \tag{30}$$

For $z_m \ll d$, this has the solution $z_m \approx z_{m_0}(t)/2$, but as $z_m$ approaches $d$, the time dependence is much weaker and $z_m^2 \approx z_{m_0}^2(t)[1 - \rho_m/\rho_l]$. Accordingly, we estimate that the flow has penetrated through most of the lithosphere [i.e. $z_m(t) \approx d$] after the elapse of a time $t_p$ given by

$$t_p = \frac{d}{v_r}\left[\frac{6\eta v_r}{(\rho_l - \rho_m)g d^2}\right]^{1/3} \tag{31}$$

$$\Rightarrow t_p \approx (5 \times 10^5 \text{ yr})\left(\frac{30 \text{ mm yr}^{-1}}{v_r}\right)^{2/3}\left(\frac{\eta}{10^{19} \text{ Pa s}}\right)^{1/3}. \tag{32}$$

The estimate for $t_p$ is larger by $(\cos\theta)^{-4/3}$ for a non-vertical conduit. As time progresses, $z_{m_0}(t)$ continues to grow, and the height of the flow exceeds $d$. At sufficiently long times (actually not much longer than $t_p$), the flow rises to a height $h_0 = (\rho_l/\rho_m - 1)d$ above the upper surface of the old lithosphere. This provides the hydrostatic head for a lateral flow.

Two conclusions from Schubert & Garfunkel's (1984) study of leaky transforms are relevant here. One is their estimate of 20–30 MPa for the tensile stress required to overcome the viscous resistance to filling the crack. This is an order of magnitude smaller than the typical applied stress at failure in our models, thus the dynamics will not be significantly affected by this resistance. Secondly, by using geological constraints on the time required to open sections of the Dead Sea and Salton Trough–Gulf of California transforms, they were able to place an upper bound of $1.5 \times 10^{20}$ Pa s on the viscosity of the upwelling mantle. If these conduits opened at a constant rate, the limit would be reduced to $10^{19}$ Pa s. We would attribute these low values to the presence of partial melt, as discussed below, and it is interesting to note that Rydelek & Sacks (1988) obtained a viscosity of $7 \times 10^{18}$ Pa s by interpreting seismicity patterns in terms of stress migration under the northeast Japan arc, clearly a region of partial melting.

One conceivable way to accommodate the head developed at the rift would be by formation of basaltic flows from pressure-release melting of mantle in the rift zone. The basalt source (expressed as a volume flux per unit length of rift) is $Fv_r d$, where $F$ is the mean degree of melting of mantle material rising into the rift. For mid-ocean ridges, $F$ is about 0.2. For our situation, $F$ is more likely to be around 0.05. The much lower estimate arises from consideration of two factors. First, the solidus is likely to be considerably shallower than the thickness of the lithosphere, so much of the upward mantle flow in the rift produces no melting at all. Second, the form of the flow is likely to be different because there need be no sharply defined ridge crest. In a broad rift zone (and assuming for the moment no mantle flooding onto the plate surface), we can expect that only a very small fraction of the upwelling material achieves shallow depths. Even with $F = 0.05$, a crustal thickness of $Fd = 5$ km could be produced, comparable to the hydrostatic head $h_0$. However, this assumes no lateral flow of the basalt. For example, a flow of thickness 10 m would be capable of propagating laterally on the order of 100 km (even in the absence of any regional slope) before cooling significantly, because of its low viscosity. Thus the most likely consequence of basaltic flooding is a broad floodplain, much wider than the rift zone and correspondingly much thinner than the hydrostatic height $h_0$.

Necessarily, the mantle will rise to the hydrostatic height, since the basalt cannot, and begin to flood the upper surface of the lithosphere. We can treat this as a gravity current with a height at the source of $h_0$. First we consider the gravity current ignoring any lithospheric flexure, as illustrated in Fig. 16. This is a well-studied situation (*cf.* Huppert 1982). The non-linear diffusion equation describing the evolution of $h(x, t)$ has the form

$$\frac{\partial h}{\partial t} = \frac{g}{3\nu}\frac{\partial}{\partial x}\left(h^3\frac{\partial h}{\partial x}\right), \tag{33}$$

where $\nu$ is the kinematic viscosity. The similarity solution for $h$ is adequately approximated for our purpose by the expression

$$h(x, t) \approx h_0\left[1 - \frac{x}{x_n(t)}\right]^{1/3}, \tag{34}$$

where $x_n$ refers to the nose of the flow;

$$x_n(t) \approx \sqrt{\frac{g h_0^3 (t - t_p)}{3\nu}} \approx (40 \text{ km})\left(\frac{10^{19} \text{ Pa s}}{\eta}\right)^{1/2}\left(\frac{t - t_p}{10^6 \text{ yr}}\right)^{1/2}. \tag{35}$$

Now let us consider the effect of the loading of this flow on the lithospheric flexure. The situation is illustrated in Fig. 17. Clearly, our simple gravity flow approximation only applies for the time during which the lithospheric deflection $w(x, t)$ (positive downwards here) is small compared with $h_0$. Quite generally, but provided the lithospheric deflection is small compared to the lithospheric *thickness*, we have the following flexure equations:

$$D\frac{\partial^4 w}{\partial x^4} = \rho_m g h(x, t), \qquad 0 < x < x_n(t), \tag{36}$$

$$D\frac{\partial^4 w}{\partial x^4} = -\rho_m g w(x, t), \qquad x > x_n(t), \tag{37}$$

$$\left.\frac{\partial^2 w}{\partial x^2}\right|_{x=0} = \left.\frac{\partial^3 w}{\partial x^3}\right|_{x=0} = 0, \tag{38}$$

$$w, \quad \frac{\partial w}{\partial x}, \quad \frac{\partial^2 w}{\partial x^2}, \quad \frac{\partial^3 w}{\partial x^3} \quad \text{continuous at } x = x_n(t), \tag{39}$$

where $D$ is the flexural rigidity. The right-hand side to eq. (36) is easily obtained by comparing the total hydrostatic pressure drop from a point on the top of the gravity current to a point vertically beneath at the base of the lithosphere with the (normal) total hydrostatic pressure rise at the centre of the rift. For $h = h_0$, this is merely the negative buoyancy of the slab, but for $h < h_0$ it is proportionately less. Of course, the right-hand side of the force balance equation is continuous

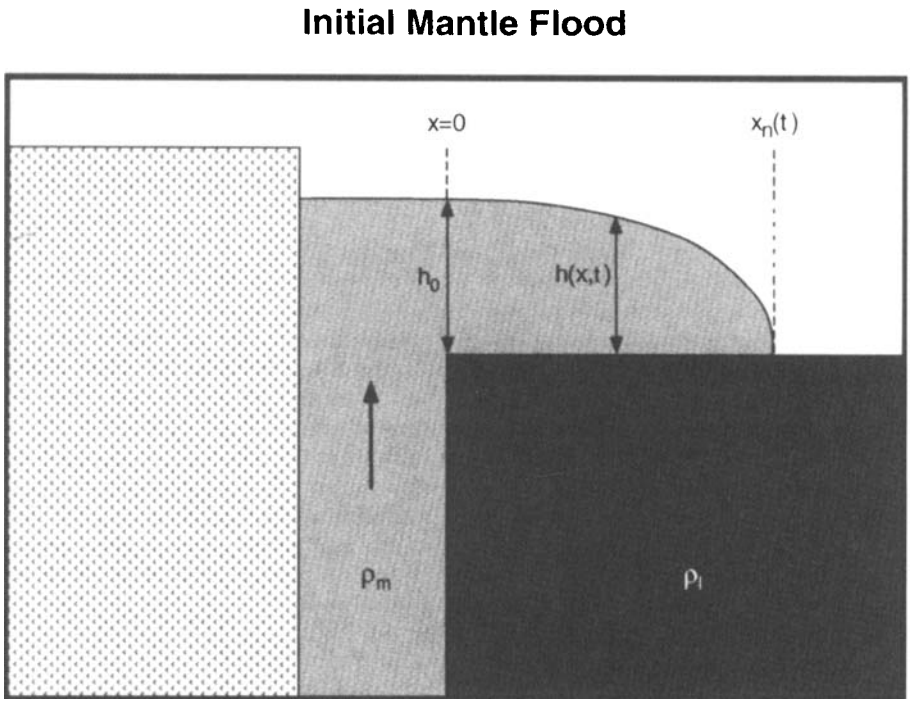


**Figure 16.** Initial mantle flood onto the oceanic plate. Static pressure drives hot mantle to a height $h_0 > 3$ km above the compensated sea-floor, comparable to the relative height of ridges. The column is laterally unsupported and so flows out in a gravity current with its nose at $x_n(t)$ and a sloping surface at $h(x, t)$.

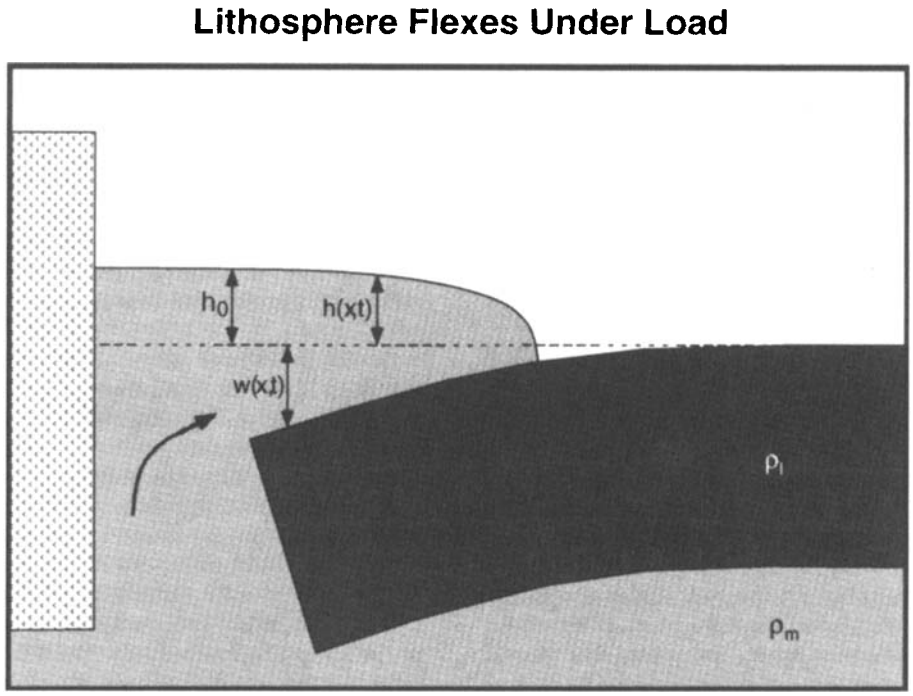


**Figure 17.** Flexural response of the lithosphere to the gravity current (not to scale). As the flow advances, the plate flexes under its load by $w(x, t)$. This increases the height of the flow channel, aiding its advance.

at $x = x_n$ since at that point, $h = -w$. The gravity current solution can be inserted into these equations and an exact solution obtained. However, it is an adequate approximation to replace the true $h(x, t)$ with the approximation $h = h_0$ for $0 < x < x_n$ and $h = 0$ for $x > x_n$. This has the virtue that it will be correct even when $w$ is no longer negligible compared with $h$. The solution to the equations then becomes:

$$w = w_0 + w_1 x + \frac{\rho_m g h_0 x^4}{24D}, \qquad x < x_n(t), \tag{40}$$

$$w = [a\cos(q\xi) + b\sin(q\xi)]e^{-q\xi}, \qquad x > x_n(t), \tag{41}$$

$$w_0 \equiv \frac{\rho_m g h_0 x_n^2(t)}{2Dq^2}\left[1 + \frac{3}{2}x_n(t)q + x_n^2(t)q^2 + \frac{1}{8}x_n^3(t)q^3\right], \tag{42}$$

$$w_1 \equiv \frac{\rho_m g h_0 x_n(t)}{2Dq^2}\left[-1 - x_n(t)q + \frac{1}{6}x_n^2(t)q^2\right], \tag{43}$$

$$a \equiv \frac{\rho_m g h_0 x_n(t)}{2Dq^3}\left[1 + \frac{1}{2}x_n(t)q\right], \tag{44}$$

$$b \equiv -\frac{\rho_m g h_0 x_n^2(t)}{4Dq^2}, \tag{45}$$

$$\xi \equiv x - x_n(t), \tag{46}$$

$$q \equiv \left(\frac{\rho_m g}{4D}\right)^{1/4}. \tag{47}$$

At the nose of the flow, the lithospheric deflection is $w(x_n) = a$, which can be rewritten (using the definition of $q$) in the illuminating form

$$w[x_n(t)] = 2h_0 x_n(t)q\left[1 + \frac{1}{2}x_n(t)q\right], \tag{48}$$

showing that the lithospheric deflection can no longer be ignored in the gravity current once $x_n(t)$ is greater than about $1/4q$. In this regime, the modified gravity current equation becomes

$$\frac{\partial(h+w)}{\partial t} = \frac{g}{3\nu}\frac{\partial}{\partial x}\left[(h+w)^3\frac{\partial h}{\partial x}\right], \tag{49}$$

$$h(0,t) = h_0, \qquad h[x_n(t),t] = -w[x_n(t),t]. \tag{50}$$

Together with the still-applicable flexural profile, this completely specifies the behaviour of $w(x,t)$. It is easy to show that once $x_n$ exceeds about $1/4q$, the gravity current accelerates dramatically because the plate subsides and provides an ever-increasing channel for the flow.

The evolution can thus be rather neatly divided into three epochs. In the first epoch ($t < t_p$), the mantle upwelling penetrates the lithosphere through a channel provided by the rift. In the second epoch ($t_p < t < t_f$) a rather thin mantle flow floods onto the top of the oceanic lithosphere, initiating the foundering. From the criterion $x_n(t) = 1/4q$, we deduce that

$$t_f \approx t_p + (2.5\times10^5\ \text{yr})\left(\frac{\eta}{10^{19}\ \text{Pa s}}\right)\left(\frac{D}{10^{23}\ \text{N m}}\right)^{1/2}. \tag{51}$$

For an effective elastic thickness of 40 km, this corresponds to a flow extending about 25 km from the rift after, with $\eta = 10^{19}$ Pa s, roughly 1 Myr. At the end of this epoch, the plate has subsided by only a few kilometres but sufficiently to provide for a much thicker channel for subsequent mantle flooding. The third epoch sees an accelerated foundering of the slab, where the motion is sufficiently large that the limiting factor will be the drag or pressure support of underlying mantle. This last regime does not seem to have any simple analytical approximation but clearly corresponds to the Stokes sinking of the slab, with velocities of the order of a few centimetres per year. The hydrodynamical pressure difference across the slab as foundering accelerates will lead to a horizontally directed force that, along with ridge push, favours closing up of the rift.

The principal issue with this scenario is whether the flooding of mantle on to old oceanic lithosphere can actually occur. This depends on the time-scale for thermal diffusion through the thickness of the flow being considerably larger than the time-scale for development of the flow, i.e.

$$\frac{h_0^2}{\kappa} > t_f - t_p \tag{52}$$

$$\Rightarrow \frac{g h_0^3 (h_0 q)^2}{\nu\kappa} \geq 1. \tag{53}$$

Notice that the criterion takes the form (not surprisingly) of a modified Rayleigh number. There is a very strong dependence on $h_0$ implied by this equation, and for values of 3 or 4 km, the criterion is only satisfied for low viscosities (less than $10^{19}$ Pa s). It must accordingly be acknowledged that the foundering of lithosphere is marginally accomplished in even the best of circumstances, *but very old lithosphere founders more readily than younger (yet negatively buoyant) lithosphere because it provides for the thickest flood.*

## 3 DISCUSSION

This model's promise for describing initiation is directly related to the decreased margin strengths relative to compressional models. The lowest shear resistance obtained by Mueller & Phillips (1991) for an old passive margin under compression was $\sim 3\times10^{13}$ N m$^{-1}$, giving an average strength of 400 MPa. The highest integrated resistance developed in any of our models is comparable: using $T_r = 800$ °C, $\mu = 0.85$, $v = 1$ nm s$^{-1}$, and the wet-mantle basal shear model, we obtain a peak value $F_r = 2.6\times10^{13}$ N m$^{-1}$, although the average strength $F_r/h$ in this case peaks at 500 MPa. Smaller peak strengths may be obtained with reasonable parameters. For example, using $T_r = 600$ °C, $\mu = 0.5$, and $v = 2$ nm s$^{-1}$ yields peak values of $F_r = 7.7\times10^{12}$ N m$^{-1}$ and $F_r/h = 204$ MPa for the wet (lowest-drag) shear model. The primary reason for the difference is that the sign change of the applied load causes it to have the opposite effect on fault strength; in a tensile model, in fact, a sufficiently large applied stress makes the frictional resistance vanish.

Obviously we have made a large number of simplifications that will affect the behaviour in detail. Among the more important ones is the margin sedimentation we omitted and the significant increase in flexural shear stresses it would cause. Previous studies of sediment-induced flexure, which assumed that the sediment-free lithosphere would be unflexed, predict shear stresses on the order of 100 MPa (e.g. Cloetingh & Wortel 1982; Cloetingh *et al.* 1989; Stein *et al.* 1989). McQueen (1986) showed that deflections (and their derivatives) are further enhanced by erosion and uplift on the continental side of the margin in southeastern Australia, although this occurrence depends on the regional topography and drainage network. An idea of how much more readily failure might occur can be obtained by reconsidering Fig. 14. If these curves are truncated at 100 MPa after allowing a 100 Myr period for sediment accumulation, we find that the margins either fail upon loading or that their failure times are advanced by 50–160 Myr. Notably, the effect is greater for the models with weak basal coupling because they approach failure more gradually. Increased flexure also favours a steeper fault, which makes the applied tension closer to fault normal, decreases the

fault length, and may ease rift formation. Sediments complicate the evolution of margin strength, however. They increase static pressures in underlying material and will, when sufficiently compacted, contribute to the frictional strength. Conversely, they provide insulation that will cause isotherms to migrate upwards through the material. The net effect on margin strength will depend on the hydrothermal circulation and the rates of burial and lithification.

A better understanding of the basal tractions is clearly desirable, as might be obtained by dynamically modelling the system shown in Fig. 2(a) and discussed in the Appendix. One dynamic consideration is that a finite driving force is available, which limits the integrated resistive traction that can be applied to the base of the plate. Although the modern Pacific plate shows that the surface area can become quite large, the time variation of the stresses depends on this dynamic balance. On the other hand, an important opportunity also exists here because our model could be used to initiate new subduction zones self-consistently in a convection calculation with a realistic temperature-dependent rheology.

Among other issues to consider, the thermal and structural evolution of the margin, beginning with the initial basin-forming rift, defines the compositional density distribution, thermal moments that will modify the flexural behaviour, and the spatial and temporal variations in density and rheological properties. Uncertainties in these must be reduced before we can hope to quantitatively predict failure in natural settings. Finally, as noted above, the foundering model presented here is only marginally viable, and thus this process merits further study. In particular, we would want a model of sufficient detail to test whether ophiolite formation and obduction could, in fact, result from our scenario.

## 4 SUMMARY AND CONCLUSIONS

Our scenario for the initiation of subduction differs markedly from previous models in that we do not envision lithospheric contraction. Due to the high strength of the lithosphere in compression, initial contraction requires unusual geometries, stresses, or tectonic events, and these make it difficult to explain the nearly complete recycling of old ocean basins. Instead, we have made use of the fact that the lithosphere is weaker in tension to build a model that predicts rift formation at passive continental margins and foundering of the old oceanic lithosphere. Although there are quantitative uncertainties, we have described generally applicable means by which the necessary deviatoric tension can arise and believe that we have demonstrated the model's mechanical plausibility.

The margin's flexural development is an important component of our model. We have considered a simple margin history in which, as reflected in stratigraphic and gravity data, subsidence of the oceanic lithosphere is flexurally inhibited by coupling to a buoyant continent. The resulting shear stresses provide a significant fraction, typically more than 25 per cent, of the total required for fault slip. The slope of the flexural profile also results in a tension that can more than offset ridge push.

The main source of margin-normal tension, however, is shear stresses on the base of the lithosphere that resist its motion away from the mid-ocean ridge. These stresses are difficult to quantify but can be particularly important: while ridge push and margin flexure (absent sedimentation) saturate for old basins, the surface area to which tractions may be applied continues to grow.

The long-term shear resistance offered by a potential fault at the margin must exceed the flexural shear stresses and shear stresses resulting from the applied tension if the continental and oceanic lithosphere are to remain coupled. We have shown that the tensile contributions to the normal stress can bring the frictional resistance below this threshold within 200–400 Myr for reasonable and even conservative parameter choices. We envision the formation of a passive rift at this stage, driven open by the basal shear tractions. The bathymetric difference between ridges and old basins implies pressures in the rift capable of driving a 3 km mantle column onto the edge of the old lithosphere, and we have shown how a gravity current can then expand onto the plate, causing it to founder and initiate subduction.

A preliminary review of observations related to initiation and passive margins is encouraging. These include the presence of oceanic forearc basement in continental arcs and the youth of ophiolites when they are obducted, both of which may be explained by rifting a margin and underthrusting the juvenile crust formed there. Boninites in ophiolite complexes and tectonites at their bases show depleted and hydrated geochemistries consistent with melting of rifted mantle lithosphere that receives volatiles from foundering oceanic crust. Also, borehole breakout data and several examples of margin-normal T-axes indicate that deviatoric tension does arise at passive margins in spite of ridge push.

## ACKNOWLEDGMENTS

This work benefited from discussions with numerous colleagues, including Peter Burgess, John Davidson, Jim Dolan, Mike Gurnis, Brad Hacker, Slava Solomatov, Joel Ita, Louis Moresi, and David Peate. Hong-Kie Thio helped us search the Harvard CMT catalogue. Thoughtful reviews were provided by S. Mueller, R. J. Phillips, and S. Stein. This work was generously supported by the James Irvine Foundation. Contribution No. 5481, Division of Geological and Planetary Sciences, California Institute of Technology.

## REFERENCES

Assumpção, M., 1992. The regional intraplate stress field in South America, *J. geophys. Res.*, **97,** 11 889–11 903.

Batchelor, G.K., 1967. *An Introduction to Fluid Dynamics,* pp. 216–227, Cambridge University Press, New York, NY.

Bird, P. & Kong, X.H., 1994. Computer simulation of California tectonics confirm very low strength of major faults, *Geol. Soc. Am. Bull.*, **106,** 159–174.

Brace, W.F. & Kohlstedt, D.L., 1980. Limits on lithospheric stress imposed by laboratory experiments, *J. geophys. Res.*, **85,** 6248–6252.

Bungum, H., Alsaker, A., Kvamme, L.B. & Hansen, R.A., 1991. Seismicity and seismotectonics of Norway and nearby continental shelf areas, *J. geophys. Res.*, **96,** 2249–2265.

Byerlee, J.D., 1978. Friction of rocks, *Pure appl. Geophys.*, **116,** 615–626.

Calmant, S., Francheteau, J. & Cazenave, A., 1990. Elastic layer thickening with age of the oceanic lithosphere: a tool for prediction of the age of volcanoes or oceanic crust, *Geophys, J. Int.*, **100,** 59–67.

Cameron, W.E., Nisbet, E.G. & Dietrich, V.J., 1979. Boninites, komatiites and ophiolitic basalts, *Nature,* **280,** 550–553.

Casey, J.F. & Dewey, J.F., 1984. Initiation of subduction zones along transform and accreting plate boundaries, triple-junction evolution,

and forearc spreading centres—implications for ophiolitic geology and obduction, in *Ophiolites and Oceanic Lithosphere,* pp. 269–290, eds Gass, I.G., Lippard, S.J., Shelton, A.W., Geol. Soc. Spec. Publ. **13,** Oxford.

Cathles, L.M., 1975. *The Viscosity of the Earth's Mantle,* Princeton University Press, Princeton, NJ.

Chamot-Rooke, N. & Le Pichon, X., 1989. Zenisu Ridge: mechanical model of formation, *Tectonophysics,* **160,** 175–193.

Chanier, F. & Ferrière, J., 1991. From a passive to an active margin: tectonic and sedimentary processes linked to the birth of an accretionary prism (Hikurangi margin, New Zealand), *Bull Soc. geol. France,* **162,** 649–660.

Chapple, W.M. & Tullis, T.E., 1977. Evaluation of the forces that drive the plates, *J. geophys. Res.,* **82,** 1967–1984.

Cloetingh, S. & Wortel, R., 1982. Finite element models of passive continental margins with implications for the initiation of subduction zones, *Geol. en Mijn.,* **61,** 281–292.

Cloetingh, S. & Wortel, R., 1986. Stress in the Indo-Australian plate, *Tectonophysics,* **132,** 49–67.

Cloetingh, S.A.P.L., Wortel, M.J.R. & Vlaar, N.J., 1982a. Evolution of passive continental margins and initiation of subduction zones, *Nature,* **297,** 139–142.

Cloetingh, S.A.P.L., Wortel, M.J.R. & Vlaar, N.J., 1982b. State of stress at passive margins and initiation of subduction zones, *Am. Assoc. Petrol. Geol. Mem.,* **34,** 717–723.

Cloetingh S.A.P.L., Wortel, M.J.R. & Vlaar, N.J., 1984. Passive margin evolution, initiation of subduction and the Wilson Cycle, *Tectonophysics,* **109,** 147–163.

Cloetingh, S., Wortel, R. & Vlaar, N.J., 1989. On the initiation of subduction zones, *Pure appl. Geophys.,* **129,** 7–25.

Cohen, C.R., 1982. Model for a passive to active continental margin transition: implications for hydrocarbon exploration, *Am. Assoc. Petrol. Geol. Mem.,* **66,** 708–718.

Coleman, R.G., 1977. *Ophiolites: Ancient Oceanic Lithosphere?,* Springer-Verlag, New York.

Davies, G.F., 1992. On the emergence of plate tectonics, *Geology,* **20,** 963–966.

Dengo, C.A. & Logan, J.M., 1981. Implications of the mechanical and frictional behavior of serpentinite to seismogenic faulting, *J. geophys. Res.,* **86,** 10 771–10 782.

Dewey, J.F., 1969. Continental margins: a model for conversion of Atlantic-type to Andean-type, *Earth planet. Sci. Lett.,* **6,** 189–197.

Dewey, J.F. & Bird, J.M., 1970. Mountain belts and the new global tectonics, *J. geophys. Res.,* **75,** 2625–2647.

Dickinson, W.R. & Seely, D.R., 1979. Structure and stratigraphy of forearc regions, *Am. Assoc. Petrol. Geol. Mem.,* **63,** 2–31.

Dietz, R.S., 1963. Collapsing continental rises: an actualistic concept of geosynclines and mountain building, *J. Geol.,* **71,** 314–333.

England, P. & Wortel, R. 1980. Some consequences of the subduction of young slabs, *Earth planet. Sci. Lett.,* **47,** 403–415.

Erickson, S.G., 1993. Sedimentary loading, lithospheric flexure, and subduction initiation at passive margins, *Geology,* **21,** 125–128.

Erickson, S.G. & Arkani-Hamed, J., 1993. Subduction initiation at passive margins: the Scotian Basin, eastern Canada as a potential example, *Tectonophysics,* **12,** 678–687.

Forsyth, D. & Uyeda, S., 1975. On the relative importance of the driving forces of plate motion, *Geophys. J. R. astr. Soc.,* **43,** 163–200.

Forte, A.M., Peltier, W.R. & Dziewonski, A.M., 1991. Inferences of mantle viscosity from tectonic plate velocities, *Geophys. Res. Lett.,* **18,** 1747–1750.

Forte, A.M., Dziewonski, A.M. & Woodward, R.L., 1993. Aspherical structure of the mantle, tectonic plate motions, nonhydrostatic geoid, and topography of the core–mantle boundary, in *Dynamics of Earth's Deep Interior and Earth Rotation,* pp. 135–166, eds Le Mouel, J.-L., Smylie, D.E. & Herring, T., AGU, Washington, DC.

Gripp, A.E., & Gordon, R.G., 1990. Current plate velocities relative to the hotspots incorporating the NUVEL-1 global plate motion model, *Geophys. Res. Lett.,* **17,** 1109–1112.

Hacker, B.R., 1994. Rapid emplacement of young oceanic lithosphere: argon geochronology of the Oman ophiolite, *Science,* **265,** 1563–1565.

Hager, B.H., 1991. Mantle viscosity: a comparison of models from postglacial rebound and from the geoid, plate driving forces, and advected heat flux, in *Glacial isostasy, Sea-level and Mantle Rheology,* pp. 493–513, eds Sabadini, R., Lambeck, K. & Boschi, E., Kluwer, Boston, MA.

Haskell, N.A., 1935. The motion of a viscous fluid under a surface load, I, *Physics,* **6,** 265–269.

Haskell, N.A., 1936. The motion of a viscous fluid under a surface load, II, *Physics,* **7,** 56–61.

Henyey, T.L., 1968. Heat flow near major strike-slip faults in central and southern California, *PhD thesis,* California Institute of Technology, CA.

Huppert, H.E., 1982. The propagation of two-dimensional and axisymmetric viscous gravity currents over a rigid horizontal surface, *J. Fluid Mech.,* **121,** 43–58.

Isacks, B.L. & Barazangi, M., 1977. Geometry of Benioff zones: lateral segmentation and downwards bending of the subducted lithosphere, in *Island Arcs, Deep Sea Trenches, and Back-Arc Basins,* pp. 99–114, eds Talwani, M. & Pitman, W.C., III, Maurice Ewing Series, **1,** AGU, Washington, DC.

Jarrard, R.D., 1986. Relations among subduction parameters, *Rev. Geophys.,* **24,** 217–284.

Karato, S. & Spetzler, H.A., 1990. Defect microdynamics in minerals and solid-state mechanisms of seismic wave attenuation and velocity dispersion in the mantle, *Rev. Geophys.,* **28,** 399–421.

Karato, S. & Wu, P., 1993. Rheology of the upper mantle: a synthesis, *Science,* **260,** 771–778.

Karig, D.E., 1982. Initiation of subduction zones: implications for arc evolution and ophiolite development, in *Trench-Forearc Geology: Sedimentation and Tectonics on Modern and Ancient Active Plate Margins,* pp. 563–576, eds Leggett, J.K., Geol. Soc. Spec. Publ., **10,** Oxford.

Karner, G.D., & Watts, A.B., 1983. Gravity anomalies and flexure of the lithosphere at mountain ranges, *J. geophys. Res.,* **88,** 10 449–10 477.

King, S.D. & Masters, G., 1992. An inversion for radial viscosity structure using seismic tomography, *Geophys. Res. Lett.,* **19,** 1551–1554.

Kroenke, L.W. & Walker, D.A., 1986. Evidence for the formation of a new trench in the Western Pacific, *EOS, Trans. Am. geophys. Un.,* **67,** 145–146.

Lachenbruch, A.H. & McGarr, A., 1990. Stress and heat flow, in *The San Andreas Fault System, California,* pp. 261–277, ed. Wallace, R.E., USGS Prof. Paper, **1515,** Washington, DC.

Langseth, M.G., Le Pichon, X. & Ewing, M., 1966. Crustal structure of mid-ocean ridges, 5, heat flow through the Atlantic ocean floor and convection currents, *J. geophys. Res.,* **71,** 5321–5355.

McAdoo, D.C. & Sandwell, D.T., 1985. Folding of oceanic lithosphere, *J. geophys. Res.,* **90,** 8563–8569.

McAdoo, D.C., Martin, C.F. & Poulouse, S., 1985. Seasat observations of flexure: evidence for a strong lithosphere, *Tectonophysics,* **116,** 209–222.

McKenzie, D.P., 1967. Some remarks on heat flow and gravity anomalies, *J. geophys. Res.,* **72,** 6261–6273.

McKenzie, D.P., 1977. The initiation of trenches: a finite amplitude instability, in *Island Arcs, Deep Sea Trenches, and Back-Arc Basins,* pp. 57–62, eds Talwani, M. & Pitman, W.C. III, Maurice Ewing Series, **1,** Washington, DC.

McKenzie, D. & Bickle, M.J., 1988. The volume and composition of melt generated by extension of the lithosphere, *J. Petrol.,* **29,** 625–679.

McNutt, M.K., 1984. Lithospheric flexure and thermal anomalies, *J. geophys. Res.,* **89,** 11 180–11 194.

McQueen, H.W.S., 1986. Vertical movements and stress across passive continental margins, *R. Soc. N. Z. Bull.,* **24,** 99–109.

Molnar, P. & Atwater, T., 1978. Interarc spreading and Cordilleran tectonics as alternates related to the age of subducted oceanic lithosphere, *Earth planet. Sci. Lett.*, **41,** 330–340.
Morrow, C.A., Shi, L.Q. & Byerlee, J.D., 1982. Strain hardening and strength of clay-rich fault gouges, *J. geophys. Res.*, **87,** 6771–6780.
Mount, V.S. & Suppe, J., 1987. State of stress near the San Andreas fault: implications for wrench tectonics, *Geology,* **15,** 1143–1146.
Mueller, S. & Phillips, R.J., 1991. On the initiation of subduction, *J. geophys. Res.*, **96,** 651–665.
Okal, E., Woods, D.F. & Lay, T., 1986. Intraplate deformation in the Samoa-Gilbert-Ralik area: a prelude to a change of plate boundaries in the Southwest Pacific?, *Tectonophysics,* **132,** 69–77.
Oxburgh, E.R. & Parmentier, E.M., 1977. Compositional and density stratification in oceanic lithosphere—causes and consequences, *J. geol. Soc. Lond.,* **133,** 343–355.
Parmentier, E.M. & Haxby, W.F., 1986. Thermal stresses in the oceanic lithosphere: evidence from geoid anomalies at fracture zones, *J. geophys. Res.*, **91,** 7193–7204.
Parsons, B. & Richter, F.M., 1980. A relation between the driving force and geoid anomaly associated with mid-ocean ridges, *Earth planet. Sci. Lett.*, **51,** 445–450.
Pearce, J.A., Lippard, S.J. & Roberts, S., 1984. Characteristics and tectonic significance of supra-subduction zone ophiolites, in *Marginal Basin Geology,* pp. 77–94, eds Kokelaar, B.P., & Howells, M.F., Geol. Soc. Spec. Publ., **16,** Oxford.
Peltier, W.R., 1989. Mantle viscosity, in *Mantle Convection,* pp. 389–478, ed. Peltier, W.R., Gordon & Breach, New York, NY.
Rabinowitz, P.D., 1982. Gravity measurements bordering passive continental margins, in *Dynamics of Passive Margins,* pp. 91–115, ed. Scrutton, R.A., Geodynamics Series, **6,** Washington, DC.
Rabinowitz, P.D. & LaBrecque, J.L., 1977. The isostatic gravity anomaly: key to the evolution of the ocean-continent boundary at passive continental margins, *Earth planet. Sci. Lett.*, **35,** 145–150.
Rydelek, P.A. & Sacks, I.S., 1988. Asthenospheric viscosity inferred from correlated land-sea earthquakes in north-east Japan, *Nature,* **336,** 234–237.
Sacks, I.S., 1983. The subduction of young lithosphere, *J. geophys. Res.*, **88,** 3355–3366.
Sandwell, D.T., 1984. Thermomechanical evolution of oceanic fracture zones, *J. geophys. Res.*, **89,** 11 401–11 413.
Sandwell, D. & Schubert, G., 1982. Lithospheric flexure at fracture zones, *J. geophys. Res.*, **87,** 4657–4667.
Schubert, G. & Garfunkel, Z., 1984. Mantle upwelling in the Dead Sea and Salton Trough–Gulf of California leaky transforms, *Ann. Geophys.*, **2,** 633–648.
Stanistreet, I.G., Kukla, P.A. & Henry, G., 1991. Sedimentary basinal responses to a Late Precambrian Wilson Cycle: the Damara Orogen and Nama Foreland, Namibia, *J. African Earth Sci.*, **13,** 141–156.
Steckler, M.S. & Watts, A.B., 1982. Subsidence history and tectonic evolution of Atlantic-type continental margins, in *Dynamics of Passive Margins,* pp. 184–196, ed. Scrutton R.A., *Geodynamics Series,* **6,** Washington, DC.
Stein, C. & Stein, S., 1992. A model for the global variation in oceanic depth and heat flow with lithospheric age, *Nature,* **359,** 123–129.
Stein, S., Cloetingh, S., Sleep, N.H. & Wortel, R., 1989. Passive margin earthquakes, stresses and rheology, in *Earthquakes at North-Atlantic Passive Margins: Neotectonics and Postglacial Rebound,* pp. 231–259, eds Gregersen, S. & Basham, P.W., *NATO ASI Ser. C,* **266,** Dordrecht, Netherlands.
Stevenson, D.J. & Turner, J.S., 1977. Angle of subduction, *Nature,* **270,** 334–336.
Tovish, A.G., Schubert, G. & Luyendyk, B.P., 1978. Mantle flow pressure and the angle of subduction: non-Newtonian corner flows, *J. geophys. Res.*, **83,** 5892–5898.
Turcotte, D.L. & Ahern, J.L., 1977. On the thermal subsidence history of sedimentary basins, *J. geophys. Res.*, **82,** 3762–3766.
Turcotte, D.L., Haxby, W.F. & Ockendon, J.R., 1977. Lithospheric instabilities, in *Island Arcs, Deep Sea Trenches, and Back-Arc Basins,* pp. 63–69, eds Talwani, M. & Pitman, W.C. III, Maurice Ewing Series, **1,** Washington, DC.
Watts, A.B., 1978. An analysis of isostasy in the world's oceans, 1, Hawaiian-Emperor seamount chain, *J. geophys. Res.*, **83,** 5989–6004.
Watts, A.B., Karner, G.D. & Steckler, M.S., 1982. Lithospheric flexure and the evolution of sedimentary basins, *Phil. Trans. R. Soc. Lond.,* A., **305,** 249–281.
Wessel, P., 1992. Thermal stresses and the bimodal distribution of elastic thickness estimates of the oceanic lithosphere, *J. geophys. Res.*, **97,** 14 177–14 193.
Wessel, P. & Haxby, W.F., 1990. Thermal stresses, differential subsidence, and flexure at oceanic fracture zones, *J. geophys. Res.,* **95,** 375–391.
Wiens, D.A. & Stein, S., 1984. Intraplate seismicity and stresses in young oceanic lithosphere, *J. geophys. Res.*, **89,** 11 442–11 464.
Wiens, D.A. & Stein, S., 1985. Implications of oceanic intraplate seismicity for plate stresses, driving forces and rheology, *Tectonophysics,* **116,** 143–162.
Wilson, J.T., 1966. Did the Atlantic close and then re-open?, *Nature,* **211,** 676–681.
Zoback, M.L., 1992. First- and second-order patterns of stress in the lithosphere: the World Stress Map project, *J. geophys. Res.*, **97,** 11 703–11 728.
Zoback, M.D. *et al.,* 1987. New evidence on the state of stress of the San Andreas fault system, *Science,* **238,** 1105–1111.
Zoback, M.L. *et al.,* 1989. Global patterns of tectonic stress, *Nature,* **341,** 291–298.
Zuber, M.T., 1987. Compression of oceanic lithosphere: an analysis of intraplate deformation in the Central Indian Basin, *J. geophys. Res.*, **92,** 4817–4825.

## APPENDIX A: GENERALIZED CORNER FLOW MODEL

Consider the following half-space model for flow induced by the surface plate motions and a vertically sinking slab. The geometry is shown in Fig. A1; note that here $x$ increases landwards from the ridge. If we consider the flows associated with the region adjacent to the subduction and the region adjacent to the ridge with stream functions $\psi_1$ and $\psi_2$, respectively, then

$$\psi_1 = \frac{v_s r}{\left(1 - \frac{4}{\pi^2}\right)}\left[-\sin\theta + \frac{2}{\pi}\theta\sin\theta + \frac{4}{\pi^2}\theta\cos\theta\right], \qquad \text{(A1)}$$

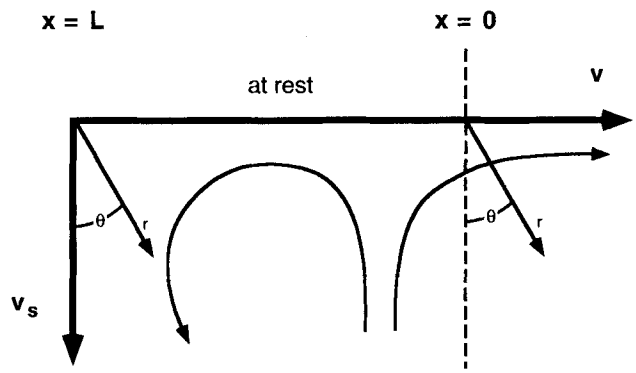


**Figure A1.** Geometry of the generalized corner-flow model. A plate taken to be at rest overlies two corner-flow regions. On the left, a slab subducts at speed $v_s$ and generates a counterclockwise circulation. On the right, a clockwise flow is generated by a ridge migrating to the right at speed $v$. Angles $\theta$ are measured counterclockwise from the vertical and $r$ is the radial distance from the respective corners.

$$\psi_2 = vr\left[\cos\theta + \frac{2}{\pi}\theta\cos\theta\right]. \tag{A2}$$

As in the usual polar coordinate representation (*cf.* Batchelor 1967), $r$ is the radial distance from the trench and ridge, respectively, while the angle $\theta$ is measured counterclockwise from the vertically downward position. If we use $z$ as the vertical distance downwards from Earth's surface, and retain only the lowest-order terms in $z$ (so as to represent the flow near the surface), then we obtain

$$\psi_1 = \frac{-4v_s z^2}{(\pi^2-4)(L-x)}, \tag{A3}$$

$$\psi_2 = \frac{2vz^2}{\pi x} \tag{A4}$$

for $0 < x < L$, with velocity components

$$v_x = -\frac{\partial\psi_{1\,\text{or}\,2}}{\partial z}, \qquad v_z = \frac{\partial\psi_{1\,\text{or}\,2}}{\partial x}. \tag{A5}$$

We now wish to construct a stream function that involves both flows and satisfies the boundary conditions. Consider the proposition

$$\psi = \psi_1 + \psi_2 + \delta\psi. \tag{A6}$$

Clearly, all the boundary conditions are satisfied, provided

$$\left.\frac{\partial\delta\psi}{\partial x}\right|_{z=0} = \left.\frac{\partial\delta\psi}{\partial z}\right|_{z=0} = 0, \tag{A7}$$

$$\left.\frac{\partial\delta\psi}{\partial x}\right|_{x=L} = -\left.\frac{\partial\psi_2}{\partial x}\right|_{x=L}; \qquad \left.\frac{\partial\delta\psi}{\partial z}\right|_{x=L} = -\left.\frac{\partial\psi_2}{\partial z}\right|_{x=L}, \tag{A8}$$

where the latter conditions are constructed so that the velocity boundary conditions on the slab surface ($x = L$, $z \ll L$) are satisfied. A perturbative solution of the form $\delta\psi \propto (a + bx)z^2$ with $a$ and $b$ constants automatically satisfies $\nabla^4\psi = 0$, so we finally obtain

$$\delta\psi = -\frac{4vz^2}{\pi L} + \frac{2vxz^2}{\pi L^2}. \tag{A9}$$

It follows that the basal shear stress for the plate is of the form

$$\tau(x) = \eta\left[\frac{8v_s}{(\pi^2-4)(L-x)} - \frac{4v}{\pi x} + \frac{8v}{\pi L} - \frac{4vx}{\pi L^2}\right], \tag{A10}$$

where $\eta$ is the dynamic viscosity. (Because $x$ increases towards the trench here, trench-directed shear stresses are considered positive, in contrast with the main text.) As is usual with corner-flow solutions, there are divergences as one approaches $x = 0$ or $x = L$. One way to treat them is to assume that $\tau(x)$ is truncated at some maximum value $\tau_m$, i.e.

$$\tau(x) = \tau_m, \qquad 0 \le x \le x_{m1} \wedge L - x_{m2} \le x \le L \tag{A11}$$

$$x_{m1} \equiv \frac{4\eta v}{\pi\tau_m}, \qquad x_{m2} \equiv \frac{8\eta v_s}{(\pi^2-4)\tau_m}. \tag{A12}$$

Finally we come to the expression for the stress within the plate for $x < L - x_{m2}$, with tensile stresses considered positive:

$$\sigma(x) = \sigma_r + \frac{\tau_m x_m}{h(x)} - \frac{\eta}{h(x)} \times \left\{\frac{8v_s}{(\pi^2-4)}\ln\left(\frac{L}{L-x}\right) - \frac{4v}{\pi}\left[\ln\left(\frac{x}{x_m}\right) - \frac{2x}{L} + \frac{x^2}{2L^2}\right]\right\}, \tag{A13}$$

where $x_m$ is, of course, the value appropriate to small $x$ (i.e. $x_{m1}$), $\sigma_r < 0$ is the stress due to ridge push, and $h$ is the thickness of the brittle/elastic layer supporting the stresses. An example of the predicted stress distribution is given in Fig. 9.